

**A SYSTEMS ANALYSIS OF THE IMPACT OF NAVIGATION
INSTRUMENTATION ON-BOARD A MARS ROVER, BASED ON A
COVARIANCE ANALYSIS OF NAVIGATION PERFORMANCE**

by

Douglas Eric Leber

**S.B., Aeronautics and Astronautics
Massachusetts Institute of Technology
Cambridge, Massachusetts (1985)**

**Submitted to the Department of Aeronautics and Astronautics
in Partial Fulfillment of the Requirements for the Degree of**

MASTER OF SCIENCE in AERONAUTICS AND ASTRONAUTICS

at the

MASSACHUSETTS INSTITUTE OF TECHNOLOGY

May 1992

© Douglas E. Leber and the Charles Stark Draper Laboratory, 1992. All Rights Reserved

Signature of Author

Department of Aeronautics and Astronautics
May 8, 1992

Certified by

Timothy J. Brand
Principal Member Technical Staff, Charles Stark Draper Laboratory
Technical Supervisor

Certified by

Stanley W. Shepperd
Principal Member Technical Staff, Charles Stark Draper Laboratory
Technical Supervisor

Certified by

Dr. Joseph F. Shea
Adjunct Professor, Department of Aeronautics and Astronautics
Thesis Advisor

Accepted by

Dr. Harold Y. Wachman
Chairman, Departmental Committee on Graduate Studies
Department of Aeronautics and Astronautics

MASSACHUSETTS INSTITUTE
OF TECHNOLOGY

JUN 05 1992

LIBRARIES

**A SYSTEMS ANALYSIS OF THE IMPACT OF NAVIGATION
INSTRUMENTATION ON-BOARD A MARS ROVER, BASED ON A
COVARIANCE ANALYSIS OF NAVIGATION PERFORMANCE**

by

DOUGLAS E. LEBER

**Submitted to the Department of Aeronautics and Astronautics
on May 8, 1992.
in partial fulfillment of the requirements for the degree of
Master of Science in Aeronautics and Astronautics**

Abstract

As part of the Space Exploration Initiative, the exploration of Mars will undoubtedly require the use of rovers, both manned and unmanned. Many mission scenarios have been developed, incorporating rovers which range in size from a few centimeters to ones large enough to carry a manned crew. Whatever the mission, accurate navigation of the rover on the Martian surface will be necessary.

This thesis considers the initial rover missions, where minimal in-situ navigation aids will be available at Mars. A covariance analysis of the rover's navigation performance is conducted, assuming minimal on-board instrumentation (gyro compass and speedometer), a single orbiting satellite, and a surface beacon at the landing site. Models of the on-board instruments are varied to correspond to the accuracy of various levels of these instruments currently available. A comparison is made with performance of an on-board IMU. Landing location and satellite orbits are also varied.

**Technical Supervisor: Timothy J. Brand
Principal Member Technical Staff,
Charles Stark Draper Laboratory**

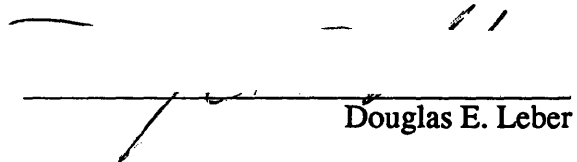
**Technical Supervisor: Stanley W. Shepperd
Principal Member Technical Staff,
Charles Stark Draper Laboratory**

**Thesis Supervisor: Dr. Joseph F. Shea
Adjunct Professor, Department of Aeronautics
and Astronautics**

Acknowledgment
May 8, 1992

This thesis was prepared at the Charles Stark Draper Laboratory, Inc., under contract NAS9-18426. Publication of this thesis does not constitute approval by Draper or the sponsoring agency of the findings or conclusions contained herein. It is published for the exchange and stimulation of ideas.

I hereby assign my copyright of this thesis to the Charles Stark Draper Laboratory, Inc., Cambridge, Massachusetts.


Douglas E. Leber

Permission is hereby granted by the author and the Charles Stark Draper Laboratory to the Massachusetts Institute of Technology to reproduce and to distribute copies of this thesis document in whole or in part.

Table of Contents

Chapter 1 Introduction	6
1.1 Rover Concepts	7
1.2 Scope	9
Chapter 2 Background.....	10
2.1 Assumptions	12
2.2 Instrumentation.....	15
2.3 Covariance Analysis Background	17
2.4 Navigation Filter	18
2.5 Variable Definitions	23
Chapter 3 Rover Models	25
3.1 Minimal Instrumentation Case	27
3.1.1 Position States	27
3.1.2 Position Error Determination	29
3.1.3 Instrument Models.....	30
3.1.3.1 Speedometer	30
3.1.3.2 Gyrocompass	32
3.1.4 The Vertical Track	32
3.1.5 Summary of Rover Error Dynamics.....	33
3.1.6 Initializing The Covariance Matrices	34
3.1.6.1 Initial Error Covariance Matrix.....	34
3.1.6.2 White Noise Covariance Matrix.....	35
3.2 Full Inertial Measurement Unit Case	38
3.2.1 Rover Position States	38
3.2.2 Velocity State	39
3.2.3 IMU Error Analysis.....	41
3.2.3.1 Position Errors.....	41
3.2.3.2 Velocity Errors.....	42
3.2.3.3 Instrument Models.....	43
3.2.3.3.1 System Alignment Errors	43
3.2.3.3.2 Gyroscope Drift.....	45
3.2.3.3.3 Accelerometer Errors	45
3.2.4 The Vertical Track	46
3.2.5 Summary of Rover Dynamics	47
3.2.6 Initial Covariance Matrices	49
3.3 Measurements.....	50
Chapter 4 Implementation	53
4.1 Minimal Instrumentation Case	54
4.1.1 Baseline	54
4.1.2 Simulation Trials	56
4.2 IMU Case	57
4.2.1 Baseline	58
4.2.2 Simulation Trials.....	58
Chapter 5 Results	60
5.1 Minimal Instrumentation Case	60
5.2 Full IMU Case.....	69
Chapter 6 Conclusions	76

Bibliography.....	78
Appendix A Notation	79
Appendix B Variable Definitions.....	82
Appendix C Values of Physical Constants.....	84

List of Tables

Table 1-1 Rover Mission Characteristics	8
Table 4-1 Baseline Profile for Minimal Instrumentation	53
Table 4-2 Baseline Variations for Minimal Instrumentation	55
Table 4-3 Baseline Profile for the IMU	57
Table 4-4 Baseline Variations for the IMU.....	57
Table 5-1 The Effect of Rover Speed on Relative Position Errors	67

List of Figures

Figure 2.1 Terrestrial Navigation Geometry	13
Figure 2.2 Definition of Trajectory Uncertainties.....	19
Figure 3.1 Definition of Coordinate Frames	25
Figure 3.2 Definition of Misalignment Angles	44
Figure 3.3 Range Measurement Geometry	51
Figure 5.1 Baseline Minimal Instrumentation Relative E/W Position Errors.....	60
Figure 5.2 Baseline Minimal Instrumentation Relative N/S Position Errors.....	61
Figure 5.3 Baseline Minimal Instrumentation Relative Vertical Position Errors	62
Figure 5.4 Baseline Minimal Instrumentation Speed Errors.....	63
Figure 5.5 Baseline Minimal Instrumentation Heading Errors	63
Figure 5.6 Minimal Instrument Rover E/W Position Error Growth	64
Figure 5.7 Minimal Instrument Rover N/S Position Error Growth.....	65
Figure 5.8 Minimal Instrument E/W Errors for ZUPs vs Range Measurements	65
Figure 5.9 Minimal Instrument N/S Errors for ZUPs vs Range Measurements	66
Figure 5.10 Baseline IMU E/W Relative Position Errors	69
Figure 5.11 Baseline IMU N/S Relative Position Errors	70
Figure 5.12 Baseline IMU Speed Errors	71
Figure 5.13 Baseline IMU Heading (Velocity Direction) Errors.....	71
Figure 5.14 IMU Rover E/W Position Error Growth.....	72
Figure 5.15 IMU Rover N/S Position Error Growth.....	73
Figure 5.16 Baseline IMU E/W Errors for ZUPs vs Range Measurements.....	74
Figure 5.17 Baseline IMU N/S Errors for ZUPs vs Range Measurements.....	74

Chapter 1: Introduction

In President Bush's July 20, 1989 speech, he indicated a specific goal of returning people to space, starting with Space Station Freedom, then returning to the moon and finally on to Mars. That speech prompted the Space Exploration Initiative and spawned the recent flurry of interest in space exploration. It also provided a challenge to NASA and the US space industry to reasonably meet those objectives with the limited resources available.

As a result, NASA Administrator Truly ordered a 90-day study¹ to look at what was needed to launch such a large program, and what the specific course of action should be, both for management and mission design. The Report of the 90-Day Study on Human Exploration of the Moon and Mars, November 1989, spells out a high level strategy for returning to the Moon and moving on to Mars. It also indicates some key technologies that must be worked on to achieve these goals. The basic strategy is to begin with simple missions to survey and characterize the Lunar and Martian environments. These will be followed by robotic missions to look more closely at selected areas on the surfaces (based on information from the preliminary missions). Next will be robotic sample return missions, also using rovers. Ultimately, manned missions will be launched with specific landing sites having been surveyed and chosen for their scientific usefulness and their appropriateness for landing a manned vehicle. Each mission is to provide a basis for the next and must be compatible with follow-on hardware and software.

To attain these successive goals, the study asserts that the Earth-based navigation systems must be expanded and a navigation infrastructure is needed at Mars. Since each successive phase will require more precise navigation information, it is reasonable to plan that precursor missions can gradually put this infrastructure in place. The use of rovers,

¹A. Cohen, "The Report of the 90-Day Study of Human Exploration of the Moon and Mars", NASA, November 1989.

both manned and unmanned is a fundamental part of the exploration of the Martian surface. Accurate navigation of the rovers will be essential, especially in site surveys for subsequent manned missions.

Cost is a major constraint, which directly affects size, weight and power requirements for any Mars mission. One of the major recommendations of the Augustine Commission's March 1990 report² was that future programs should be based on the budgets available - do what you can with what you have. It is important however to plan projects in such a way that each project, on a small scale can be scheduled, funded, and completed within a budget and contribute its part to the ultimate goal of landing man on Mars. Dr. Mike Griffin, the new Associate Director of NASA for the Space Exploration Initiative has said this is the path he plans to take. Begin with the initial surveying and Mars Observer missions, fund them completely and then move to the next phase when budgets allow. By defining "self-contained" missions on a small scale, one can avoid one of the concerns noted above - inconsistent budgets. Having one or two large programs that are underfunded is inefficient and ultimately much more costly. It is also unlikely that SEI funding will increase substantially in the near future in light of NASA's commitment to the costly shuttle program and the national budget problems.

1.1 Rover Concepts

Rovers can be very useful tools in the exploration of other planets, specifically Mars; their missions would include:

Site Characterization: measure environmental conditions of potential human landing sites using imaging and electromagnetic sounding instruments.

Long Range Traverse: locate and characterize mineralogy in the area of a potential landing site. Could be performed after site survey by same rover.

Small Rover Sample Acquisition: collect samples in a local area and return to

²N. Augustine, et. al., "Report of the Advisory Committee on the Future of the US Space Program", NASA, PB91-181529, December 17, 1990.

lander for analysis and possible return to Earth.

Large Rover Sample Acquisition: Long traverse and collection of samples over a larger area, with analysis on board. Could return to a lander, or cache samples for retrieval by subsequent missions.

Each mission has its own goals and constraints and therefore each requires a slightly different rover design. A Jet Propulsion Laboratory study³ conducted in 1989 categorized various rovers by their missions. Table 1-1 summarizes the conclusions.

Table 1-1: Rover Mission Characteristics

Rover Size	Range/Life	Mission	Comments
Micro (1-3 kg)	10's of meters a few days	-local sample collection -survey small sites, imaging & top soil characterization	-many "ants" deployed -low reliability -minimal on-board computation
Mini (100 kg)	100 meters 150 days	-site characterization, remote sensing, some digging -local sample collection	- no night operations - up to 60 samples collected in 150 days - samples selected using lander imaging - rover dependent on lander for power, commanding and communications
Small (300 kg)	5 km 150 days	- site characterization, remote sensing - small scale construction demo - sample collection and return	- no night ops - longer traverse, but fewer samples collected - own power system, less dependence on lander - lower data rate transmission to lander at farther distances
Large (500- 1000 kg) Simple	10 km 1500 days	- site characterization and long traverse mineralogy identification - sample collection from larger area	- Simple mission, no Mars comm orbiter - Sophisticated direct to Earth comm needed - limited operations due to comm restrictions

³D.S. Pivrotto and W.C. Dias, "United States Planetary Rover Status - 1989", NASA/JPL, JPL Publication 90-6, May 15, 1990.

Large (500-1000 kg) Moderate	100 km 1500 days	<ul style="list-style-type: none"> - diverse sample collection - large range general survey - surface drilling, deeper sampling 	<ul style="list-style-type: none"> - order of 10 times faster turn around on commanding needed over simple rover to get range - direct to Earth and imaging orbiter relay comm, rover has sophisticated antenna pointing - Assumes some foreknowledge of site from precursor imaging mission (Viking order resolution)
Large (500-1000 kg) Capable	1000 km 1500 days	<ul style="list-style-type: none"> - regional characterization and sampling - subsurface sounding - preliminary construction and excavation evaluation 	<ul style="list-style-type: none"> - Dedicated comm satellite expected in Martian orbit for relay to Earth, simple omni antenna on rover - High resolution foreknowledge of site expected (from precursor imaging orbiter) - landing site accuracy to 1 km

1.2 Scope

The cost and sizing constraints expected for any Mars mission will, of course, affect rovers and their subsystems, including onboard navigation instrumentation. This thesis explores possible minimal navigation instrumentation packages that could be used onboard a Mars rover to provide semi-autonomous operation capability for the rover, requiring minimal support from Earth based control centers. Based on the previous Mars beacon survey work performed at the Charles Stark Draper Laboratory (CSDL), a model was developed for a rover moving on the Mars surface. Onboard navigation instrumentation provided the navigation for the rover between expected passes from a communication satellite in Mars orbit, when more accurate position measurements could be taken from the satellite. A covariance analysis was performed to provide an initial determination as to the feasibility of using the instrumentation packages chosen. A comparison of navigation performance was performed between using only a speedometer and gyrocompass (minimal instrumentation), and using a full IMU.

Chapter 2: Background

Many studies have been performed both at the Charles Stark Draper Laboratory (CSDL) and the Jet Propulsion Laboratory (JPL) regarding navigation of spacecraft and surface rovers at Mars. JPL has based its studies on utilizing the Deep Space Network for most mission navigation requirements, with some use of autonomous systems to augment the DSN. Their rover navigation studies rely heavily on the JPL concept of controlling the rover movements from the Earth⁴. Stereo images would be sent from the rover via a landing craft or satellite to the Earth, where they would be analyzed to determine the best course for the rover to take. Commands would then be relayed to the rover for it to maneuver on a short (few meters) trajectory before it would stop and send another set of images to the Earth control team. This process, though effective, is not entirely efficient. The time delay in communications can be as much as forty minutes, and the time required to analyze the images and prepare the commands is expected to be several hours. It is likely that only one or two traverses (of just a few meters) could be expected in a days time.

Studies at Draper include Mars aerocapture navigation performance and surface beacon survey accuracy analyses, both relying on onboard systems to perform the navigation functions. The beacon survey studies used a covariance analysis approach and relied on a satellite in orbit around Mars. The studies concentrated on determining survey accuracies attainable from taking radiometric range and Doppler measurements from the satellite to beacons on the planet surface. These relative measurements between the satellite and beacons were found to be insufficient to determine the actual longitude of the beacons being surveyed, though the longitudinal position relative to the satellite was determined very accurately. By supplementing the radio measurements with some

⁴Ibid, and, F. Sturms, et.al., "Concept for a Small Mars Sample Return Mission Using Microtechnology", NASA/JPL, JPL Publication D-8822, October 1991.

optical measurements, the absolute longitude could be found. This was done with a star tracker to align an IMU on the satellite with a distant star, and then locate the beacon optically. Assuming a hemispheric mirror or corner cube at the beacon site, the angle between the star and the beacon could be determined by the IMU. Though dust storms could create problems for the optical measurements in the long term, the beacon survey problem was of short duration.

The studies also showed that two-way range measurements were more effective than Doppler measurements, providing location accuracy of a few meters after only a couple of days with satellite passes approximately every two hours. The actual performance varied with the geometry provided by orbit of the satellite and the location of the beacon⁵. The range measurements provided very good accuracy in the directions along track of the satellite motion and vertical to the satellite path; cross track information was not as accurate. For instance, a satellite flying in an equatorial (0° inclination) orbit over a beacon on the equator would not be able to determine the North/South position of the beacon very accurately since it is not observable from the satellite. The variable geometry between the beacon and overflying satellite provides information in the other two directions. By varying the inclination of the orbits and the latitude of the beacon, much better accuracy in the North/South direction was attainable.

These studies indicate that similar navigation accuracy (on the order of meters) would be attainable for a rover traversing the Martian surface. In the time between satellite passes, the rover would navigate autonomously using onboard systems until its position was determined more accurately by satellite range measurements. The rover missions would be of longer duration than the survey studies, thus prohibiting effective use of optical measurements. For the rover navigation problem, however, the relative position between the rover and a Home Base or landing site is more important than the actual rover position. It can be assumed that the landing site would be surveyed using the

⁵T.J. Brand and S.W. Shepperd, "Candidate Mars Local Navigation Infrastructures", AAS 91-496, AAS/AIAA Astrodynamics Specialist Conference, August 19, 1991.

star tracker measurements and then the rover could navigate relative to the landing site making the rover position error highly correlated with that of the base. These beacon survey studies, therefore, were the basis for the covariance study performed in this rover navigation study.

2.1 Assumptions

To perform the feasibility study for navigation performance, the mission constraints were identified and several assumptions were made to establish the scope of the navigation requirements. The Martian environment places several physical constraints on the problem. Its atmosphere is thin but turbulent, and prone to frequent dust storms. The dust storms particularly limit the usefulness of optical sensing and measuring instrumentation. The temperature also changes drastically from day to night, with variations between 160° and 260° Kelvin. The planet rotation rate is equivalent to that of Earth, but the gravity is only about a third of Earth's. The distance of Mars from Earth causes a communications delay of from 5 to 40 minutes, depending on the orbital phases of the two planets.

The mission to be performed by the rover was assumed to be that of site characterization with some local sample collection. The rover was assumed to be small to medium in size and unmanned. It, as well as the landing craft, would be equipped with an omni antenna permitting range measurements to the orbiter. The rover will move at modest speed, probably under 0.1 meters per second, and the mission will be of limited duration and distance from the landing craft.

The area to be surveyed by the rover is assumed to have been imaged to a resolution of a few meters, either by a precursor imaging orbiter mission or from images taken by the landing craft on its decent. The rover's course will be commanded through a trajectory of speed and heading, and onboard sensors are available to detect and avoid unexpected obstacles.

Two-way range measurements to the landing craft and the rover will be taken from a satellite, presumed to be needed for communications relay anyway. Since a direct field of view between the rover and landing craft can not be guaranteed, no direct measurements between the two were allowed. The only other external measurement is a zero velocity update (ZUP), taken by default when the rover stops. The rover stopping provides 'perfect' information as to the rover's planet relative velocity, and is thus an excellent measurement. The onboard navigation instruments are assumed to be taking continuous measurements and are treated as error sources to the rover velocity uncertainty in the covariance analysis.

Navigating a vehicle on a planet surface is primarily a two dimensional problem, as variations in altitude will be small over the short distances expected to be traveled. The requirement for navigation accuracy is to avoid surface hazards and to allow a rover to return to the Home Base or landing site. If base location is known in relation to the surface hazards, then the navigation accuracy of the rover relative to the base is important. Thus there is no requirement for high accuracy absolute location knowledge. Clearly, the most important information needed to determine position is the distance traveled from the base and the heading taken.

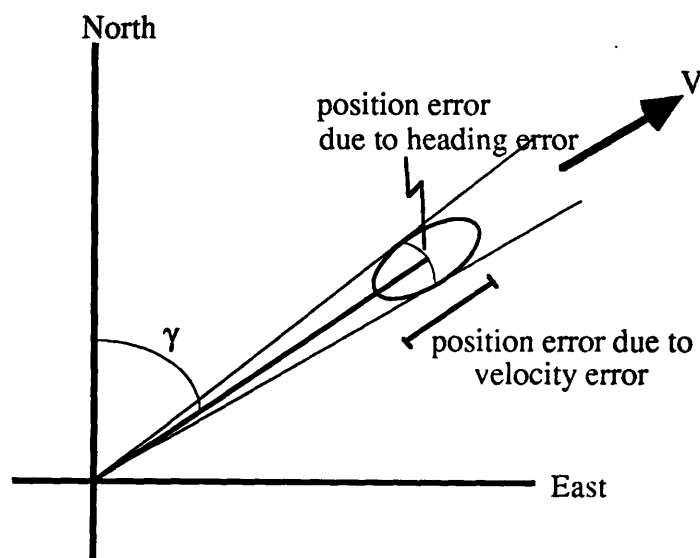


Figure 2.1: Terrestrial Navigation Geometry

Figure 2.1 shows the path of the rover, assumed to be traveling at constant speed (v) and heading (γ). A rough calculation can be made of the relative affects of the speed and heading error contributions to the position error. The vertical motion (altitude change) can be represented in terms of the pitch angle of the rover, providing the third velocity component. The changes in pitch, and therefore altitude, will be small, since the rover is assumed to be traveling on fairly level terrain. The error contribution of the pitch angle is then negligible (second order along the direction of motion) compared to the position error contributions from speed and heading. At a given time, t , the rover has traveled a distance $d = v t$. The error in the direction of motion, δd , is based on the measuring device used, such as an odometer, and can be assumed to be scaled based the actual distance traveled, due to on wheel irregularities, contraction and expansion, and slippage. The heading error, $\delta\gamma$, can be assumed to be a bias for this initial consideration of the problem, based on not having exact knowledge of the direction of North (i.e. compass inaccuracy). The heading errors to contribute state errors perpendicular to the path of motion. These errors can be resolved in the North and East directions, assuming some initial errors at the starting point:

$$\delta N = dN_0 + \delta\gamma d \sin\gamma + \delta d \cos\gamma$$

$$\delta E = dE_0 + \delta\gamma d \cos\gamma + \delta d \sin\gamma$$

Substituting $\delta d = d SF$, where SF is the scale factor of the distance measurement, the equations become:

$$\delta N = \delta N_0 + d\gamma d \sin\gamma + d SF \cos\gamma$$

$$\delta E = \delta E_0 + d\gamma d \cos\gamma + d SF \sin\gamma$$

It is clear that the position errors could depend greatly on initial conditions if they are large, but the growth in errors is due equally to errors in knowledge of heading and errors in measurement of distance traveled.

2.2 Instrumentation

For most autonomous navigation missions, an inertial measurement unit (IMU) is used. An IMU is comprised of three single-degree-of-freedom (or two two-degree-of-freedom) gyroscopes and three accelerometers. The gyroscopes provide a stable orthogonal reference frame and the accelerometers measure all sensed accelerations (or specific forces) acting on the vehicle. Known forces which are acting on the rover, such as the contact force due to gravity, can be subtracted from the accelerometer readings providing the relative vehicle accelerations in the IMU platform reference frame. The translational motion of the vehicle can then be determined. Highly accurate IMU's have been developed and could be used on rover missions, but the components can be very expensive. Less accurate IMU's may not be adequate due to the gravity environment of a planet surface. Since IMUs are very expensive and can make demands on the power and computational resources of the vehicle, it is desirable to find a simpler, less expensive set of instruments that could provide comparable navigation accuracy.

For instance, the navigation requirements can be fulfilled by a simple compass and odometer, which measure the two important quantities needed for terrestrial navigation. Since Mars has no appreciable magnetic field (less than 0.03% that of Earth's⁶) a magnetic compass would not be useful. A gyro compass could be used, however, since the rotation rate of Mars is almost the same as the Earth's. Such instruments have been widely used in Earth terrestrial navigation, both on ships and in aircraft, for many years. They are reliable and inexpensive, though they are not as accurate as the gyroscopes used in spacecraft quality IMU's.

⁶T.A. Mutch, et.al., "The Geology of Mars", Princeton University Press, Princeton, NJ, 1976, pp29-30.

A gyrocompass is a two degree of freedom gyroscope which has its spin axis pointed horizontally in the direction of North (or the positive horizontal component of the spin axis of the planet). A pendulous mass provides a continuous torque causing the gyroscope spin axis to precess about the direction of North as the planet rotates. This motion is Schuler tuned (damped) so that in its steady state the spin axis nominally points North in the horizontal plane, to an accuracy on the order of $0.5^{\circ 7}$. This accuracy should be adequate for a slow moving rover on the Mars surface, but there is a drawback to the gyrocompass; it is not useful near the polar regions. Obviously, the North direction in the horizontal plane is ill-defined in the polar regions. As the equatorial regions are the most likely places for initial exploration, this issue should not affect the use of a gyrocompass on the rover mission being studied.

The measurement of distance can be done simply and inexpensively with an odometer. An extra, unpowered wheel can be provided on the rover, with an instrument to count rotations and thus determine distance traveled, knowing the wheel circumference. As our heading will be changing with time, we must measure distance traveled relative to the previous heading change, or effectively measure speed. By taking time differences of the odometer measurements, speed can be determined, thus, in effect, making the instrument a speedometer. For that reason, a speedometer, rather than an odometer, was chosen for the minimal instrument case. The instruments are actually the same, with the speedometer requiring some computational capabilities to perform the time differencing.

Another possible instrument complement was also considered, but not modeled. This option uses gyroscopes to provide heading reference and two accelerometers to provide an indication of the horizontal. The accelerometers basically act as (and could be replaced with) an inclinometer, merely detecting the direction of the gravity vector, and thus do not have to be very accurate. Translational motion would still be determined by a

⁷W. Wrigley, W.A. Hollister, and W.G. Denhard, "Gyroscopic Theory, Design and Instrumentation", The MIT Press, Cambridge, MA, 1969, pp 187-209.

speedometer. Three gyroscopes would still be required to align the IMU system. Though the accuracy requirement for the accelerometers would be greatly reduced and thus less expensive than the full IMU, this system is more costly and complicated than the minimal instrument case and could only increase the heading accuracy, based on the accuracy of the gyroscopes used.

2.3 Covariance Analysis Background

Covariance analysis is a statistical tool which provides visibility into the feasibility of a proposed system or operation. For navigation, one assumes a nominal, or expected, trajectory, but that trajectory is subject to errors. Thus, the actual trajectory, or instantaneous position and velocity of the vehicle, will differ from the nominal and this difference can be represented statistically. Definitions of the various statistical terms follow⁸:

probability - the limit, as the number of trials in a random experiment becomes large, of the ratio of the number of times an event occurs to the total number of trials.

random variable, X - a variable that can take on values at random, or the outcome of a random experiment.

probability density function, $f(x)$ - a function representing the probability of each result of a random experiment.

mean value (or expectation), $E[X] = \bar{X} = \int x f(x) dx$ - the sum of all values a random variable may take (all outcomes of a random experiment) weighted by the probability of occurrence. The first moment of X.

mean squared value, $E[X^2] = \bar{X^2} = \int x^2 f(x) dx$ - second moment of X, the square root of which is called the root mean squared value.

variance, $\sigma^2 = \bar{X^2} - \bar{X}^2 = \int (x - \bar{X})^2 f(x) dx$ - the mean squared deviation from the

⁸A. Gelb, Editor, "Applied Optimal Estimation", The MIT Press, Cambridge, MA, 1974, pp27-34.

mean. The square root, σ , is the standard deviation from the mean.

covariance - gives an indication of the degree to which two random variables, X and Y, are correlated. It is the expectation of the product of the deviations of the two random variables from their means: $E[(X-E[X])(Y-E[Y])] = E[XY] - E[X] E[Y]$

correlation coefficient, ρ - covariance normalized by the standard deviations of X and Y, $\rho = \frac{E[XY] - E[X] E[Y]}{\sigma_x \sigma_y}$. If X and Y are independent, ρ is zero,

indicating that the variables are uncorrelated. The range of ρ is from -1 to 1, where either extreme indicates 100% correlation.

The nominal, or assumed, trajectory determines the mean position and velocity at any time, with the actual state being represented as a random variable that can take on values around this mean. It is usually assumed that the probability density function of the actual vehicle state uncertainties is Gaussian.

2.4 Navigation Filter

Covariance analysis is based on a linearized perturbation model of the system and any external measurements of the system. Dynamics of the system are determined and the error characteristics of the various measurement types are modeled. The error covariance is integrated with time, based on the dynamics models, and a Kalman filter is used to update the covariance matrix when a measurement is taken. The measurements provide new information, allowing a better estimation of the actual vehicle state.

There are two important aspects to covariance analysis, propagating the states and covariance matrix with time and recursively updating the matrix when a new measurement is taken. The following explanation of the Kalman filtering technique will use a spacecraft as an example. The result will be equally applicable to the overall filter for the rover navigation problem, as will be explained in Chapter 3.

Linearized perturbation techniques are used to describe the vehicle dynamics, where the estimated state is assumed to deviate by a small quantity from the nominal state. Figure 2.2 indicates the nominal reference trajectory, assumed to be conic, and the estimated trajectory being flown.

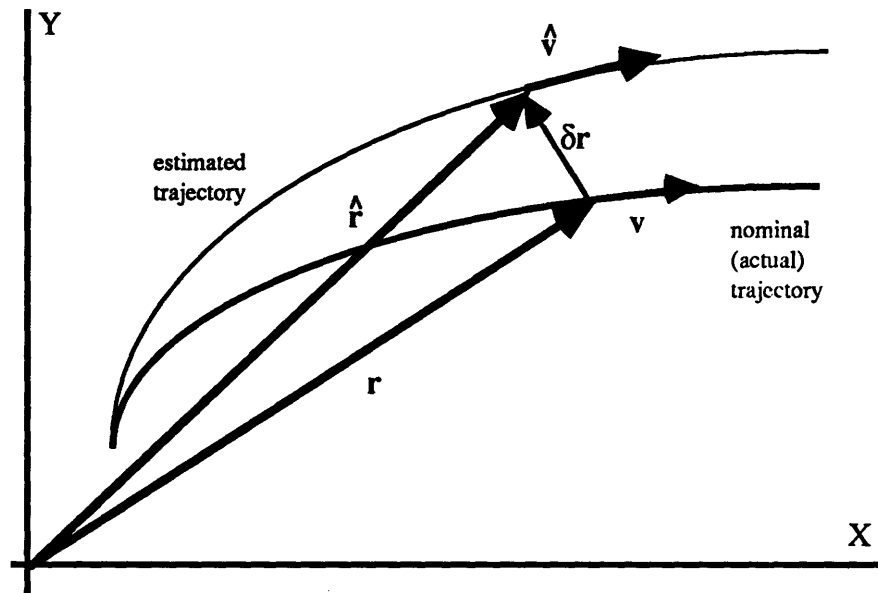


Figure 2.2: Definition of Trajectory Uncertainties

The estimated position and velocity states can be represented in terms of the nominal reference states and the error, or perturbation, between the two:

$$\hat{\mathbf{r}} = \mathbf{r} + \delta\mathbf{r} \quad (2.1)$$

$$\hat{\mathbf{v}} = \mathbf{v} + \delta\mathbf{v} \quad (2.2)$$

and

$$\hat{\mathbf{x}}_s = \mathbf{x}_s + \delta\mathbf{x}_s \quad (2.3)$$

where \mathbf{x}_s is a six component vector defining the total state of the satellite reference trajectory (\mathbf{x} is the total state of the satellite, rover, base problem, defined in Chapter 3):

$$\mathbf{x}_s = \begin{bmatrix} \mathbf{r} \\ \mathbf{v} \end{bmatrix}$$

It is assumed that the real state error dynamics is well approximated by the error dynamics about the nominal conic orbit. Then the dynamics of the state uncertainties can be expressed in partitioned matrix form as:

$$\delta \dot{\mathbf{x}}_s = \begin{bmatrix} \mathbf{0} & \mathbf{I} \\ \mathbf{G} & \mathbf{0} \end{bmatrix} \delta \mathbf{x}_s = \mathbf{F}_S \delta \mathbf{x}_s \quad (2.4)$$

Where \mathbf{I} is the 3x3 identity matrix and \mathbf{G} is the linearized gravity gradient matrix and is a function of time (not explicitly, but because position is a function of time):

$$\mathbf{G} = \frac{\partial \mathbf{g}}{\partial \mathbf{r}} = \frac{\mu}{r^3} [3 \frac{\mathbf{r} \mathbf{r}^T}{r^2} - \mathbf{I}]$$

where the value of \mathbf{G} is calculated at the reference position. The expression given here is for a spherical body (conic) gravitation field.

A state transition matrix, $\Phi(t, t_0)$, can be defined to describe how the state uncertainties propagate from some initial condition to the current time, specifically:

$$\delta \mathbf{x}_s(t) = \Phi(t, t_0) \delta \mathbf{x}_s(t_0) \quad (2.5)$$

At time $t = t_0$, $\Phi(t_0, t_0) = \mathbf{I}$ and the state transition matrix would propagate in the same way as the state uncertainties themselves, from equation 2.4:

$$\frac{d\Phi(t, t_0)}{dt} = \mathbf{F}_S \Phi(t, t_0) \quad (2.6)$$

An estimate of the state uncertainties can be achieved through external measurements, such as taking a position fix by measuring the angle between a star and a near body. The actual measurement will differ from what the measurement would be expected on the nominal trajectory by a small quantity:

$$\delta\tilde{q} = q_{\text{nom}} - q_{\text{meas}} \quad (2.7)$$

The nominal value can be calculated from the presupposed trajectory and subtracted from the measured value taken. Assuming scalar measurements, each measurement estimates a component (or combination of components) of the spacecraft state along some direction in position/velocity space based on the type of measurement taken. It can be shown⁹ that to first order, the uncertainty in the measurement is related to the state uncertainties by this so called measurement geometry vector, \mathbf{b} :

$$\delta q = \mathbf{b}^T \delta \mathbf{x}_s \quad (2.8)$$

A measured value will always differ from the true value by a small amount due to instrument error, thus producing a small error in the estimate of the state uncertainties from the reference:

$$\delta\tilde{q} = \delta q + \alpha \quad (2.9)$$

$$\hat{\delta \mathbf{x}}_s = \delta \mathbf{x}_s + \epsilon \quad (2.10)$$

If no measurements are taken, then the assumption is that the vehicle is on the nominal trajectory and the state uncertainties grow due to the dynamics from

⁹R.H. Battin, "An Introduction to the Mathematics and Methods of Astrodynamics", AIAA Press, New York, NY, 1987, pp 627-632.

equation 2.4. A matrix of the covariances of the state uncertainties can be defined:

$$\mathbf{E} = \mathbf{\epsilon} \mathbf{\epsilon}^T$$

With these definitions, an algorithm can be determined to propagate the error covariance matrix with time and update it when new measurements are made. The error in estimation of the state deviations is assumed to have the same dynamics as the state itself, therefore, from the definition of the covariance matrix:

$$\mathbf{E}(t_n) = \mathbf{\Phi}(t_n, t_{n-1}) \mathbf{E}(t_{n-1}) \mathbf{\Phi}(t_n, t_{n-1})^T + \mathbf{N} \quad (2.11)$$

where \mathbf{N} is process noise integral added to the error covariance matrix to account for unmodeled error sources. For computational purposes, it is easier to consider the rate of change of the error covariance matrix in terms of the state error dynamics:

$$\dot{\mathbf{\epsilon}} = \mathbf{F} \mathbf{\epsilon} \quad \text{and} \quad \dot{\mathbf{\epsilon}}^T = \mathbf{\epsilon}^T \mathbf{F}^T$$

then

$$\dot{\mathbf{\epsilon}} \mathbf{\epsilon}^T = \dot{\mathbf{\epsilon}} \mathbf{\epsilon}^T + \mathbf{\epsilon} \dot{\mathbf{\epsilon}}^T$$

and

$$\dot{\mathbf{E}} = \mathbf{F} \mathbf{E} + \mathbf{E} \mathbf{F}^T + \mathbf{Q} \quad (2.12)$$

Where \mathbf{Q} is the process noise of the system and is usually modeled as white noise acting on the velocity. Equation 2.12 can be integrated directly without the need to maintain the state transition matrix or compute the difficult process noise integral term, \mathbf{N} .

Assuming optimal estimation, when a new measurement is taken, the updated error covariance (+) matrix can be represented as a function of the covariance matrix before the measurement (-), the measurement geometry vector, and the variance of the

measurement error (α^2)¹⁰:

$$\mathbf{E}_+ = \mathbf{E}_- - \mathbf{E}_- \mathbf{b} (\alpha^2 + \mathbf{b}^T \mathbf{E}_- \mathbf{b})^{-1} \mathbf{b}^T \mathbf{E}_- \quad (2.13)$$

or, more simply,

$$\mathbf{E}_+ = (\mathbf{I} - \mathbf{w} \mathbf{b}^T) \mathbf{E}_-$$

where

$$\mathbf{w} = \frac{1}{a} \mathbf{E}_- \mathbf{b} \quad \text{and } a = \alpha^2 + \mathbf{b}^T \mathbf{E}_- \mathbf{b}$$

Once the dynamics of the system are established, the error covariance matrix can be integrated with time from equation 2.12. Measurement updates can be made by implementing equation 2.13, knowing the measurement error and the measurement geometry vector (based on the measurement type).

2.5 Variable Definitions

The navigation problem for this thesis includes the above analysis for the satellite in addition to the position error states for the beacon and the rover position, velocity and navigation instrument error states. Two states are also included to estimate the range measurement biases. For the analysis, the dynamics, error covariance and white noise matrices must be determined. They can be defined as submatrices of the various systems, where \mathbf{F}_s is the dynamics of the satellite in orbit, F_p is a scalar dynamics of the range measurement error (same for both rover and base), $\mathbf{F}_b = 0$ since the base is assumed stationary on the planet, and \mathbf{F}_R represents the rover position, velocity and instrument dynamics. The initial error covariance and white noise components can similarly be defined, substituting \mathbf{E} and \mathbf{Q} for \mathbf{F} .

¹⁰Ibid, pp 648-651.

$$F = \begin{bmatrix} F_s & 0 & 0 & 0 & 0 \\ 0 & F_p & 0 & 0 & 0 \\ 0 & 0 & F_B & 0 & 0 \\ 0 & 0 & 0 & F_p & 0 \\ 0 & 0 & 0 & 0 & F_R \end{bmatrix}$$

For the satellite states, F_s was defined in equation 2.4. The gravity gradient can be given in local navigation coordinates (East, Up, South) as:

$$G^n = \frac{\partial g^n}{\partial r^n} = \frac{\mu}{r^3} \begin{bmatrix} -1 & 0 & 0 \\ 0 & 2 & 0 \\ 0 & 0 & -1 \end{bmatrix}$$

The initial error covariance matrix values for the satellite are the initial errors in position and velocity, determined by assuming reasonable values for an orbiting satellite. Process noise is also included for the satellite velocity error states. For the Home Base, there are no dynamics, as mentioned, nor any process noise. The initial error covariances are determined as the squares of the initial errors in latitude, longitude and altitude. These will be variable parameters to be chosen in the simulation. The range measurement error states will be discussed in Chapter 3.

Chapter 3: Rover Models

There are three coordinate frames of importance (shown in Figure 3.1), the inertial frame (i) with its origin at the planet center, the planet fixed frame (m) with the same origin, and the local navigation frame (n), which is defined as positive in the East, Up and South directions. For the first order covariance study, the planet is assumed to be spherical, which makes the n-frame the local geographic frame as well.

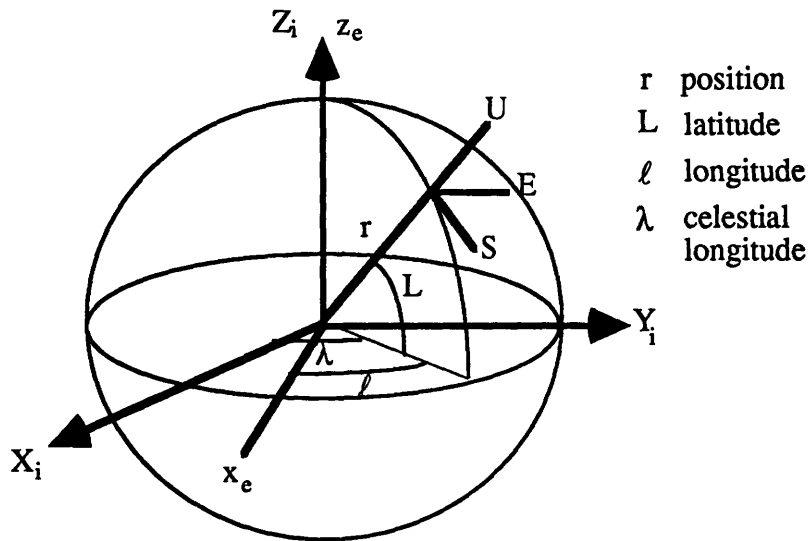


Figure 3.1: Definition of Coordinate Frames

With the coordinate frames defined, the rotation rates between frames was determined next. The angular velocity of the Mars frame with respect to the inertial frame is (in both inertial and local navigation coordinates)

$$\omega_{im}^i = \begin{vmatrix} 0 \\ 0 \\ \omega \end{vmatrix} \quad \omega_{im}^n = \begin{vmatrix} 0 \\ \omega \sin L \\ -\omega \cos L \end{vmatrix}$$

and the angular velocity of the navigation frame with respect to the Mars frame is:

$$\omega_{mn}^n = \begin{vmatrix} -\dot{L} \\ \dot{\ell} \sin L \\ -\dot{\ell} \cos L \end{vmatrix}$$

The relationship between the celestial and planet longitudes can most easily be given through their rates:

$$\dot{\ell} = \dot{\lambda} - \omega \quad (3.1)$$

Coordinate transformations can also be defined between the frames:

$$\begin{aligned} M_m^i &= \begin{vmatrix} \cos \omega t & \sin \omega t & 0 \\ -\sin \omega t & \cos \omega t & 0 \\ 0 & 0 & 1 \end{vmatrix} \\ M_n^i &= \begin{vmatrix} -\sin \lambda & \cos \lambda \cos L & \cos \lambda \sin L \\ \cos \lambda & \sin \lambda \cos L & \sin \lambda \sin L \\ 0 & \sin L & -\cos L \end{vmatrix} \\ M_n^m &= \begin{vmatrix} -\sin \ell & \cos \ell \cos L & \cos \ell \sin L \\ \cos \ell & \sin \ell \cos L & \sin \ell \sin L \\ 0 & \sin L & -\cos L \end{vmatrix} \end{aligned}$$

and the transformation from the navigation frame to latitude, longitude and altitude components is:

$$\mathbf{M}_n^{LLA} = \begin{vmatrix} 0 & 0 & -\frac{1}{R_m+h} \\ \frac{1}{(R_m+h) \cos L} & 0 & 0 \\ 0 & 1 & 0 \end{vmatrix}$$

3.1 Minimal Instrumentation Case

3.1.1 Position States

As with determining the satellite error propagation, the rover position errors must be derived in terms of their drivers, which are the velocity state errors. The rover velocity errors are, in turn, driven by the instruments which measure the velocity components (unlike the satellite velocity errors which are a function of the gravitation potential and the satellite position errors).

Convenient coordinates were chosen to efficiently track a rover on a planetary surface. The position state was maintained in latitude, longitude and altitude in planet-fixed coordinates and the velocity state included speed and heading reflecting the instrumentation to be used and the driving error sources. The rover pitch angle completed the velocity state and drove the altitude errors. The following choice of variables was used in the analysis, where the errors are defined as the difference between the actual state and the reference state ($\hat{\mathbf{x}} = \mathbf{x} + \delta\mathbf{x}$):

$\mathbf{x} =$	L	Latitude	$\delta\mathbf{x} =$	δL	Latitude error
	ℓ	Longitude		$\delta\ell$	Longitude error
	h	Altitude		δh	Altitude error
	v	Speed		δv	Speed error
	γ	Heading		$\delta\gamma$	Heading error
	α	Pitch		$\delta\alpha$	Pitch error

The position can also be expressed in either the inertial or navigation (East, Up, South)

frames, where $r = (R_m + h)$:

$$\mathbf{r}^i = \begin{bmatrix} r \cos L \cos \lambda \\ r \cos L \sin \lambda \\ r \sin L \end{bmatrix} \quad \mathbf{r}^n = \begin{bmatrix} 0 \\ r \\ 0 \end{bmatrix}$$

And similarly for the velocity:

$$\mathbf{v}^n = \begin{bmatrix} v \cos \alpha \sin \gamma \\ v \sin \alpha \\ -v \cos \alpha \cos \gamma \end{bmatrix}$$

$$\mathbf{v}^i = \begin{bmatrix} v \sin \alpha \cos \lambda \cos L - v \cos \alpha \sin \gamma \sin \lambda - v \cos \alpha \cos \gamma \cos \lambda \sin L \\ v \sin \alpha \sin \lambda \cos L + v \cos \alpha \sin \gamma \cos \lambda - v \cos \alpha \cos \gamma \sin \lambda \sin L \\ v \sin \alpha \sin L + v \cos \alpha \cos \gamma \cos L \end{bmatrix}$$

Taking the inertial derivative of position:

$$\dot{\mathbf{r}}^i = \begin{bmatrix} \dot{r} \cos \lambda \cos L - r \sin L \cos \lambda \dot{L} - r \cos L \sin \lambda \dot{\lambda} \\ \dot{r} \sin \lambda \cos L - r \sin L \sin \lambda \dot{L} + r \cos \lambda \cos L \dot{\lambda} \\ \dot{r} \sin L + r \cos L \dot{L} \end{bmatrix}$$

where $\dot{r} = \dot{h} = v \sin \alpha$

The derivative of the inertial position can then be equated to the inertial velocity. The following three independent equations result representing the dynamics of the rover position state:

$$\dot{L} = \frac{v \cos \alpha \cos \gamma}{R_m + h} \quad (3.2)$$

$$\dot{\lambda} = \frac{v \cos \alpha \sin \gamma}{(R_m + h) \cos L} \quad (3.3)$$

$$\dot{h} = v \sin \alpha \quad (3.4)$$

3.1.2 Position Error Determination

The next step in the analysis is to determine the linearized error contributions. In the linearized analysis, it is assumed that the actual state and the idealized state differ by a small error ($\hat{\mathbf{x}} = \mathbf{x} + \delta\mathbf{x}$) and that both states will propagate in the same way, so the actual state, $\hat{\mathbf{x}}$, propagates as follows, from equations 3.2 through 3.4 and the longitude relationship from 3.1:

$$\frac{d(L+\delta L)}{dt} = \frac{(v+\delta v) \cos(\alpha+\delta\alpha) \cos(\gamma+\delta\gamma)}{R_m+h+\delta h}$$

$$\frac{d(\ell+\delta\ell)}{dt} = \frac{(v+\delta v) \cos(\alpha+\delta\alpha) \sin(\gamma+\delta\gamma)}{(R_m+h+\delta h) \cos(L+\delta L)} - \omega$$

$$\frac{d(h+\delta h)}{dt} = (v+\delta v) \sin(\alpha+\delta\alpha)$$

It should be noted that the longitude equation is now in terms of the planet fixed longitude and the planet rotation rate, ω , is assumed to be known perfectly. These equations can be expanded, ignoring the higher order error terms, to give the linearized propagation equations for the rover position state error:

$$\delta\dot{L} = \frac{\cos\alpha \cos\gamma}{R_m+h} \delta v - \frac{v \cos\alpha \sin\gamma}{R_m+h} \delta\gamma - \frac{v \sin\alpha \cos\gamma}{R_m+h} \delta\alpha - \frac{v \cos\alpha \cos\gamma}{(R_m+h)^2} \delta h \quad (3.5)$$

$$\begin{aligned} \delta\dot{\ell} = & \frac{\cos\alpha \sin\gamma}{(R_m+h) \cos L} \delta v + \frac{v \cos\alpha \cos\gamma}{(R_m+h) \cos L} \delta\gamma - \frac{v \sin\alpha \sin\gamma}{(R_m+h) \cos L} \delta\alpha \\ & - \frac{v \cos\alpha \sin\gamma}{(R_m+h)^2 \cos L} \delta h + \frac{v \cos\alpha \sin\gamma \tan L}{(R_m+h) \cos L} \delta L \end{aligned} \quad (3.6)$$

$$\delta\dot{h} = v \cos\alpha \delta\alpha + \sin\alpha \delta v \quad (3.7)$$

The rover position errors are dependent largely on the actual course taken by the rover so the covariance analysis must include a model of the speed and heading of the rover. It is clear from the above equations that the contribution to the rover position errors from the pitch error will average to zero over time since the terms are proportional to $\sin\alpha$. It is assumed that the rover will be traversing a regularly undulating terrain, traveling downhill and uphill for approximately the same net time, and the maximum pitch angle is limited by the rover's ability to climb, certainly less than 10 degrees. A nominal 'trajectory' for pitch was chosen to simplify the analysis; specifically the nominal pitch, pitch rate and altitude are all assumed identically zero (the rover is traveling in the horizontal plane). The rover position errors then reduce to:

$$\dot{\delta L} = \frac{\cos\gamma}{R_m} \delta v - \frac{v \sin\gamma}{R_m} \delta\gamma - \frac{v \cos\gamma}{R_m^2} \delta h \quad (3.8)$$

$$\dot{\delta \ell} = \frac{\sin\gamma}{R_m \cos L} \delta v + \frac{v \cos\gamma}{R_m \cos L} \delta\gamma - \frac{v \sin\gamma}{R_m^2 \cos L} \delta h + \frac{v \sin\gamma \tan L}{R_m \cos L} \delta L \quad (3.9)$$

$$\dot{\delta h} = v \delta\alpha \quad (3.10)$$

As expected, these equations are all functions of the errors in the velocity state, which in turn will be a function of the instruments measuring them.

3.1.3 Instrument Models

The minimal instrument complement was determined to be a speedometer and a gyrocompass, measuring two of the previously defined velocity states.

3.1.3.1 Speedometer

The speedometer is assumed to be a simple device which counts wheel revolutions and differentiates to determine speed. The error in speed was assumed to be driven primarily by a scale factor error in the wheel dimension, taking into account

expansion and contraction of the wheel circumference due to heating and cooling. Wheel slippage will be accounted for with additional white noise, q_s , added to the time rate-of-change of the speed error.

$$\delta \dot{v} = SF_v v \quad (3.11)$$

To account for this heating and cooling cycle, the scale factor was modeled as an exponentially correlated random variable (first order Markov process). A Markov process is a statistical random process generated by passing white noise through a simple filter. The probability distribution for the process at any time is dependent only on the value immediately in the past and can be represented by the differential equation¹¹:

$$S\dot{F}_v = -\frac{1}{\tau_v} SF_v + q_v \quad (3.12)$$

The time constant, τ_v , is the correlation time of the process, when the variance has reached the $(1/e)$ of the 1σ point (one standard deviation from the nominal). For the speedometer scale factor, the time constant is reflective of the planet's day/night cycle where heating and cooling is expected to shrink and expand the wheel, thus changing the scale factor. The white noise, q_v , is chosen to bound the scale factor value. The model basically assumes that the variance of the scale factor can have any value from zero to some upper bound, which will be reached in the steady state. This value could be estimated by taking measurements; but between measurements, the variance would drive back up to its limit at a rate based on the time constant.

The time rate of change of the velocity error can be expressed in terms of the speedometer scale factor and noise due to slippage:

¹¹ A. Gelb, Editor, "Applied Optimal Estimation", The MIT Press, Cambridge, MA, 1974, pp 42-45.

$$\dot{\delta v} = \left(\dot{v} - \frac{v}{\tau_v} \right) SF_v + vq_v + q_s \quad (3.13)$$

3.1.3.2 Gyrocompass

The gyrocompass, as described previously, provides a constant heading reference from North in the horizontal plane. Having two degrees of freedom, it effectively measures the tilt of the rover (relative to North) as well. There are several error sources in the gyrocompass heading measurement:

- gyroscope drift rate
- vehicle velocity measurement
- gyroscope torquer uncertainties
- East-gyro leveling error (about the North axis)

The dominant error source is the East-gyro leveling error, with the others having lesser affect on the heading error. A simple model, which has been used in other studies¹², is to model the heading error directly as a first order Markov process:

$$\dot{\delta \gamma} = -\frac{1}{\tau_\gamma} \delta \gamma + q_\gamma \quad (3.14)$$

3.1.4 The Vertical Track

A specific measurement of the rover pitch or altitude rate is not required, as the linearized analysis of the horizontal position errors are not affected by pitch errors. Since the navigation problem is primarily two dimensional, the change in altitude was assumed to be fairly small and thus the errors in knowledge of that altitude should also be small.

¹² Kriegsmann, B. et al, "Deep Ocean Mine Site Navigation System Evaluation Final Report", Draper Laboratory, R-1049, January 1977, pp 22-26.

The vertical track was modeled separately from the in-plane motion.

The pitch errors drive the altitude errors and the two are therefore coupled. Obviously, the altitude error should be bounded. Thus, a second order Markov process for the altitude error was used to model the coupling of the altitude and pitch errors. Whereas in a first order Markov process the autocorrelation function drops off sharply with time, in the second order process the autocorrelation function has a slope of zero at the initial conditions so that the function drops off more gradually at first and then more quickly¹³. This makes sense for the terrain model, which is expected to be very smooth and not vary greatly between points not too far apart. Again, the white noise was then chosen to drive the altitude errors.

$$\ddot{\delta h} + 2\left(\frac{2.146}{\tau_\alpha}\right)\dot{\delta h} + \left(\frac{2.146}{\tau_\alpha}\right)^2 \delta h = q_\alpha \quad (3.15)$$

Taking the derivative of equation 3.10:

$$\dot{\delta h} = v \dot{\delta \alpha} + \delta \alpha \dot{v} \quad (3.16)$$

Substituting equation 3.16 into equation 3.15 and solving for $\dot{\delta \alpha}$ gives:

$$\dot{\delta \alpha} = -\left(\frac{1}{v} \dot{v} + \frac{4.292}{\tau_\alpha}\right) \delta \alpha - \frac{(2.146)^2}{v \tau_\alpha^2} \delta h + \frac{q_\alpha}{v} \quad (3.17)$$

3.1.5 Summary of Rover Error Dynamics

The time rate of change of the rover error state is now completely defined and the dynamics matrix for the rover state, F_R , is:

¹³A. Gelb, Editor, "Applied Optimal Estimation", The MIT Press, Cambridge, MA, 1974, pp 42-45.

δL	0	0	$-\frac{v \cos \gamma}{R_m^2}$	$\frac{\cos \gamma}{R_m}$	$-\frac{v \sin \gamma}{R_m}$	0	0
$\delta \ell$	$\frac{v \sin \gamma \tan L}{R_m \cos L}$	0	$-\frac{v \sin \gamma}{R_m^2 \cos L}$	$\frac{\sin \gamma}{R_m \cos L}$	$\frac{v \cos \gamma}{R_m \cos L}$	0	0
δh	0	0	0	0	0	v	0
δv	0	0	0	0	0	0	$\dot{v} - \frac{v}{\tau_v}$
$\delta \gamma$	0	0	0	0	$-\frac{1}{\tau_\gamma}$	0	0
$\delta \alpha$	0	0	$-\frac{(2.146)^2}{v \tau_a^2}$	0	0	$-\frac{\dot{v}}{v} - \frac{4.292}{\tau_a}$	0
SF_v	0	0	0	0	0	0	$-\frac{1}{\tau_v}$

3.1.6 Initializing The Covariance Matrices

With the dynamics matrix established, the next step is to determine the error covariance and the noise matrices for the rover models.

3.1.6.1 Initial Error Covariance Matrix

The initial error covariance matrix is based on the initial errors of the states of the filter and is then propagated as described in Section 2.4. It is assumed that none of the initial errors are correlated, so the error covariance matrix will initially be diagonal.

Since we are assuming that the mean of the estimation errors are zero, then the variance

of each initial estimation error term is simply the square of the initial state uncertainty. Also, since there are no correlations initially, all covariances are initially zero. The portion of the total covariance matrix, E_0 , that represents the rover states is , $E_R =$:

$$\begin{vmatrix} \delta L_0^2 & 0 & 0 & 0 & 0 & 0 & 0 \\ 0 & \delta \ell_0^2 & 0 & 0 & 0 & 0 & 0 \\ 0 & 0 & \delta h_0^2 & 0 & 0 & 0 & 0 \\ 0 & 0 & 0 & \delta v_0^2 & 0 & 0 & 0 \\ 0 & 0 & 0 & 0 & \delta \gamma_0^2 & 0 & 0 \\ 0 & 0 & 0 & 0 & 0 & \delta \alpha_0^2 & 0 \\ 0 & 0 & 0 & 0 & 0 & 0 & \sigma_{sf}^2 \end{vmatrix}$$

It is assumed that there is a Home Base, the location of which is included in the filter. Since it is likely that this base will be the landing craft delivering the rover, the initial position errors of the base and the rover will be identical and will be highly correlated. Thus, initial off diagonal terms must be included in initializing the error covariance matrix to account for the correlation. Since $E_B = E_{RR}$, where E_{RR} represents the variance submatrix of the three rover position states only, and both are diagonal matrices of the initial error variances, then $E_{RR}^T = E_{RR}$ as well, and:

$$E_{BR} = \begin{vmatrix} E_B & 0.9999 E_{RR} \\ 0.9999 E_{RR}^T & E_{RR} \end{vmatrix}$$

3.1.6.2 White Noise Covariance Matrix

The noise matrix, Q , must also be initialized. This is usually assumed to be a constant matrix, but the values may be changed as conditions change during the mission. The rover latitude and longitude error states are assumed to have no direct noise sources

as they are driven by the velocity states where the noise is incorporated. The first component of velocity error is the scalar speed error, which is driven by a scale factor. As seen previously, the scale factor was modeled as a first order Markov process with the dynamics expressed in equation 3.14. A Gaussian distribution is assumed for the scale factor and the associated white noise, so the variance of the scale factor noise, Q_v , can be represented in terms of the variance of the scale factor and the correlation time. Since in the steady state, the covariance matrix of the scale factor will be constant, then from equation 2.16:

$$\dot{\mathbf{E}} = \mathbf{0} = \mathbf{F} \mathbf{E} + \mathbf{E} \mathbf{F}^T + \mathbf{Q}$$

For a the scale factor, a scalar quantity, this is simply:

$$Q_v = \frac{2\sigma_{sf}^2}{\tau_v}$$

which is merely the variance representing the noise term, q_v , from the dynamics, since the assumption is for a zero mean error.

The speed error is affected by this noise as well, and the covariance noise terms can be determined from:

$$\begin{bmatrix} \dot{\delta v} \\ S\dot{F}_v \end{bmatrix} = \begin{bmatrix} 0 & v - \frac{v}{\tau_v} \\ 0 & \frac{1}{\tau_v} \end{bmatrix} \begin{bmatrix} \delta v \\ SF_v \end{bmatrix} + \begin{bmatrix} vq_v + q_s \\ q_v \end{bmatrix}$$

or the noise vector can be expressed as:

$$\begin{bmatrix} vq_v + q_s \\ q_v \end{bmatrix} = \begin{bmatrix} 0 & v \\ 0 & 1 \end{bmatrix} \begin{bmatrix} 0 \\ q_v \end{bmatrix} + \begin{bmatrix} q_s \\ 0 \end{bmatrix}$$

And, where Q_s is the variance representing the noise term q_s , the noise variance matrix for the speed error and speedometer scale factor states is:

$$\begin{bmatrix} v^2 Q_v & v Q_v \\ v Q_v & Q_v \end{bmatrix} + \begin{bmatrix} Q_s & 0 \\ 0 & 0 \end{bmatrix}$$

Since the gyrocompass error was also modeled as a Markov process, its noise variance term can be similarly determined:

$$Q_\gamma = \frac{2\sigma_{\gamma_0}^2}{\tau_\gamma}$$

The altitude error state is coupled with the pitch error state via a second order Markov process. The altitude errors are assumed bounded so the error covariance will reach a steady state. Assuming there is only noise in the pitch error state (which will drive the altitude error state), equation 2.16, for the altitude and pitch error states in steady state becomes:

$$\begin{bmatrix} 0 & 0 \\ 0 & 0 \end{bmatrix} = \begin{bmatrix} 0 & 1 \\ -\frac{(2.146)^2}{v \tau_\alpha^2} & -\frac{\dot{v}}{v} - \frac{4.292}{\tau_\alpha} \end{bmatrix} \begin{bmatrix} \sigma_h^2 & \sigma_{\alpha h}^2 \\ \sigma_{h\alpha}^2 & \sigma_\alpha^2 \end{bmatrix} + \begin{bmatrix} \sigma_h^2 & \sigma_{\alpha h}^2 \\ \sigma_{h\alpha}^2 & \sigma_\alpha^2 \end{bmatrix} \begin{bmatrix} 0 & -\frac{(2.146)^2}{v \tau_\alpha^2} \\ 1 & -\frac{\dot{v}}{v} - \frac{4.292}{\tau_\alpha} \end{bmatrix} + \begin{bmatrix} 0 & 0 \\ 0 & Q_\alpha \end{bmatrix}$$

This can be expanded, giving an expression for the white noise in terms of either the altitude error variance or the pitch error variance:

$$Q_\alpha = 2\left(\frac{\dot{v}}{v} + \frac{4.292}{\tau_\alpha}\right) \sigma_\alpha^2 = 2\left(\frac{\dot{v}}{v} + \frac{4.292}{\tau_\alpha}\right) \left(\frac{2.146}{v \tau_\alpha}\right)^2 \sigma_h^2$$

Since altitude is to be bounded, a reasonable altitude bias can be determined and the noise can be calculated based on the initial variance of the bias. The initial pitch variance can then be determined from the noise value. Specific values will be determined in Chapter 4.

In summary, the three rover position error states have zero noise contributions. For the rover velocity error states, the noise covariance matrix, Q_R , is:

$$\begin{array}{l|cccc}
 \text{speed error} & v^2 \frac{2\sigma_{SF}^2}{\tau_v} + Q_s & 0 & 0 & v \frac{2\sigma_{SF}^2}{\tau_v} \\
 \text{heading error} & 0 & \frac{2\sigma_{\gamma_0}^2}{\tau_\gamma} & 0 & 0 \\
 \text{pitch error} & 0 & 0 & 2\left(\frac{\dot{v}}{v} + \frac{4.292}{\tau_\alpha}\right) \left(\frac{2.146}{v \tau_\alpha}\right)^2 \sigma_h^2 & 0 \\
 \text{scale factor} & v \frac{2\sigma_{SF}^2}{\tau_v} & 0 & 0 & \frac{2\sigma_{SF}^2}{\tau_v}
 \end{array}$$

3.2 Full Inertial Measurement Unit Case

As a comparison to the minimal system, a full IMU, with three gyroscopes and three accelerometers was analyzed. An IMU measures inertial acceleration which is then integrated to give translational motion with gyroscopes to provide a stable reference frame. Since the measurements are inertial and taken in a rotating coordinate frame, the derivation of the rover motion must be treated accordingly.

3.2.1 Rover Position States

The rover position on the planet surface is best represented in the planet-fixed (Mars) coordinate frame, r^m . The navigation will be performed in the navigation frame, however, thus a transformation is required:

$$\mathbf{r}^n = \mathbf{M}_m^n \mathbf{r}^m$$

The derivative of the position in the navigation frame, which is rotating with respect to the planet fixed frame, is:

$$\mathbf{v}^n = \mathbf{M}_m^n \dot{\mathbf{r}}^m + \boldsymbol{\omega}_{mn}^n \times \mathbf{r}^n$$

or

$$\dot{\mathbf{r}}^n = \mathbf{v}^n - \boldsymbol{\omega}_{mn}^n \times \mathbf{r}^n \quad (3.18)$$

For the IMU case, the East, Up, South components of position and velocity in the navigation frame were maintained rather than latitude, longitude, and altitude. The altitude rate was assumed to be nominally zero, making the problem two dimensional in the navigation frame.

3.2.2 Velocity State

The accelerometer output is proportional to the specific forces sensed by the accelerometers in the IMU platform frame. The platform frame is assumed to be aligned with the navigation frame, so the IMU dynamics analysis was done in the more convenient navigation frame. The accelerometers measure the inertial acceleration of the vehicle and the reaction forces due to gravity:

$$\mathbf{f}^n = \mathbf{M}_i^n \ddot{\mathbf{r}}^i - \mathbf{g}^n \quad (3.19)$$

To model gravity, a spherical planet is assumed, making the gravitational field:

$$\mathbf{g}^i = -\frac{\mu}{r^2} \mathbf{i}_r \quad \text{or} \quad \mathbf{g}^n = -\frac{\mu}{r^2} \mathbf{i}_U$$

The gravity field is defined as the gravitation less the centripetal acceleration:

$$\mathbf{g}^n = \mathbf{g}^n - \boldsymbol{\omega}_{im}^n \times (\boldsymbol{\omega}_{im}^n \times \mathbf{r}^n) \quad (3.20)$$

For the linearized error model, this equation must be expressed in terms of a first derivative of the local velocity, rather than the second derivative of position. The velocity in the navigation frame can be defined as:

$$\mathbf{v}^n = \mathbf{M}_m^n \dot{\mathbf{r}}^m \quad (3.21)$$

where, from the Theorem of Coriolis:

$$\dot{\mathbf{r}}^m = \mathbf{M}_i^m (\dot{\mathbf{r}}^i - \boldsymbol{\omega}_{im}^i \times \mathbf{r}^i) \quad (3.22)$$

and

$$\mathbf{v}^n = \dot{\mathbf{r}}^n - \boldsymbol{\omega}_{mn}^n \times \mathbf{r}^n \quad (3.23)$$

The velocity from equation 3.21 can be differentiated, using the expressions in 3.22 and 3.23, to arrive at:

$$\dot{\mathbf{v}}^n = \mathbf{M}_i^n [\ddot{\mathbf{r}}^i - (\boldsymbol{\omega}_{mn}^i + 2\boldsymbol{\omega}_{im}^i) \times (\mathbf{M}_n^i \mathbf{v}^n) - \boldsymbol{\omega}_{im}^i \times (\boldsymbol{\omega}_{im}^i \times \mathbf{r}^i)] \quad (3.24)$$

Solving equation 3.24 for $\ddot{\mathbf{r}}^i$ and then substituting this into equation 3.18 gives:

$$\mathbf{f}^n = \mathbf{M}_i^n [\mathbf{M}_n^i \dot{\mathbf{v}}^n + (\boldsymbol{\omega}_{mn}^i + 2\boldsymbol{\omega}_{im}^i) \times (\mathbf{M}_n^i \mathbf{v}^n) + \boldsymbol{\omega}_{im}^i \times (\boldsymbol{\omega}_{im}^i \times \mathbf{r}^i)] - \mathbf{g}^n \quad (3.25)$$

Simplifying equation 3.25 and using 3.20, the following basic navigation equation is determined:

$$\dot{\mathbf{f}}^n = \dot{\mathbf{v}}^n + (\boldsymbol{\omega}_{mn}^n + 2\boldsymbol{\omega}_{in}^n) \times \mathbf{v}^n - \mathbf{g}^n \quad (3.26)$$

3.2.3 IMU Error Analysis

The next step is to perform the error analysis. There are two standard approaches, the Psi and Phi methods. The Phi method assumes that the navigation frame is centered at the true position of the vehicle, as previously done in the analysis. The Psi approach assumes that the navigation frame is centered at the estimated position of the vehicle, and is also called the computer frame. The computer frame is an artificial frame that represents the frame with which the computer thinks the vehicle is actually aligned; it would be the true navigation frame if the vehicle was where the computer expected it to be. In that frame, it can be assumed that the angular rates of the navigation frame with respect to the planet frame, $\boldsymbol{\omega}_{mn}$, and the rate of the planet frame with respect to the inertial frame, $\boldsymbol{\omega}_{in}$, are known without error. Both methods produce the same position error results, and the velocity errors can be converted through a transformation from one frame to the other¹⁴. For the low speed of the rover, the velocity errors should not differ significantly between the methods either. The Psi approach was chosen for this study since it was easier to implement and the position errors are of prime interest.

3.2.3.1 Position Errors

With the assumptions that the actual state and the estimated state propagate in the same manner and that the angular rates between the frames are known without error, then the rover position error rate can be obtained from equation 3.18:

$$\delta \dot{\mathbf{r}}^n = \delta \dot{\mathbf{v}}^n - \boldsymbol{\omega}_{mn}^n \times \delta \mathbf{r}^n \quad (3.27)$$

¹⁴D.O. Benson, Jr., "A Comparison of Two Approaches to Pure-Inertial and Doppler-Inertial Error Analysis", IEEE Transactions on Aerospace and Electronic Systems, Vol AES-11, No. 4, July 1975.

3.2.3.2 Velocity Errors

As in the previous case, the velocity errors are driven by the instrument errors.

The velocity error rate equation, from equation 3.26 is:

$$\delta \dot{\mathbf{v}}^n = \delta \mathbf{f}^n - (\boldsymbol{\omega}_{mn}^n + 2\boldsymbol{\omega}_{im}^n) \times \delta \mathbf{v}^n + \delta \mathbf{g}^n \quad (3.28)$$

The components of the equation are determined from the IMU model and a model for gravity errors.

The gravity, defined in equation 3.20, includes the centripetal acceleration due to the planet rotation and is sometimes called the plumb-bob gravity. There are two sources of error in the gravity term. One is errors due to deflections of the vertical, caused by the shape and mass distribution of the planet. The other error is due to the position error.

The Psi method assumes that the navigation frame is centered at the estimated location of the vehicle, therefore the assumed gravity vector differs from the true gravity vector by a small quantity.

In the ideal case, the gravitation sensed by the accelerometers would be exactly canceled out by the computed gravitation. Because of the IMU misalignments, there will be an error in the accelerometer output due to the gravitation not canceling exactly. This error will be much greater than any error caused by deflections of the vertical gravitation vector, so these gravitation errors were not modeled.

The gravity error due to rover position error, or the gravity gradient, is obtained from equation 3.20 and the definition of \mathbf{g} :

$$\delta \mathbf{g}^n = -\frac{\mu}{r^3} \delta \mathbf{r}^n + 3\frac{\mu}{r^5} \mathbf{r}^n \delta r - \boldsymbol{\omega}_{im}^n \times (\boldsymbol{\omega}_{im}^n \times \delta \mathbf{r}^n) \quad (3.29)$$

The first two terms are the gravity gradient, where δr is the altitude error. The last term is the error in centripetal acceleration which is very small compared to the gravity gradient and is usually included in modeling the vertical deflection errors. It is included here since

those errors are not modeled.

3.2.3.3 Instrument Models

The IMU is assumed to be gimballed and aligned with the navigation frame, and torqued to maintain the alignment. There are several error sources in the system that must be considered¹⁵:

- System misalignment errors

- Accelerometer non-orthogonality errors

- Gyroscope drift

- Accelerometer errors

- Platform torquing errors

- Gravity anomalies and deflections of the vertical

The accelerometer non-orthogonality errors account for the accelerometers not being placed in a true orthogonal configuration. These and the platform torquing errors were considered small compared to the others, and therefore not modeled for this study. If a strapdown IMU were used, some additional error sources would be introduced. These would be small compared to the primary errors listed above and, therefore, were not modeled in this initial analysis. Both strapdown and gimballed systems provide the same information only in different coordinate frames, so the results of this study will be indicative of a strapdown IMU as well as a gimballed one.

3.2.3.3.1 System Alignment Errors

The system misalignment is due to the gyroscopes not exactly aligning the IMU platform frame with the navigation frame. They are small angles, defined as rotation angles about an axis, as described by Figure 3.2:

¹⁵K.R. Britting, "Inertial Navigation Systems Analysis", Wiley-Interscience- a Division of John Wiley & Sons, Inc., New York, NY, 1971, pp 86-88.

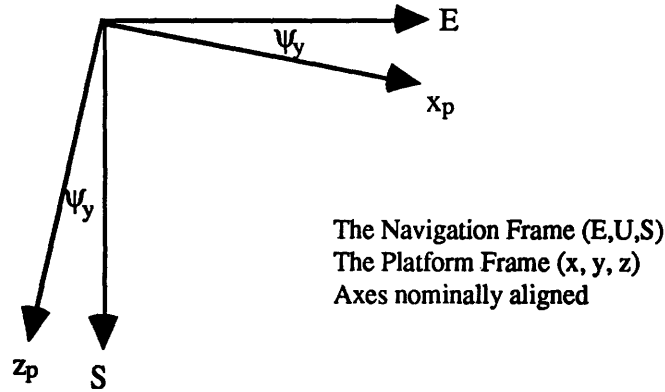


Figure 3.2: Definition of Misalignment Angles

The three misalignments are usually represented as a vector, Ψ . The effect of the misalignments is on the output of the accelerometers. Since the platform is expected to be aligned with the navigation frame, the vehicle acceleration is determined based on this assumption. An error in alignment will therefore result in errors in the components of acceleration (and ultimately velocity and position as well). The transformation between the navigation and platform frames is:

$$\mathbf{M}_n^p = \begin{bmatrix} 1 & \psi_z & -\psi_y \\ -\psi_z & 1 & \psi_x \\ \psi_y & -\psi_x & 1 \end{bmatrix} = \mathbf{I} - [\Psi \times]$$

Since the platform is assumed to be torqued to stay aligned with the navigation frame, then the rotation rate of the platform with respect to inertial coordinates, ω_{ip} , is nominally equal to ω_{in} . The alignment is subject to gyro drift rates, however, so the platform is rotating with respect to the navigation frame:

$$\omega_{ip}^p = \omega_{in}^n + \mathbf{v} \quad (3.30)$$

where \mathbf{v} is a vector representing the drift rates about each axis. The time rate of change of the misalignments, $\dot{\Psi}$ is:

$$\dot{\Psi} = \dot{\omega}_{np}^p = \dot{\omega}_{ip}^p - \dot{\omega}_{in}^p = \dot{\omega}_{ip}^p - M_n^p \dot{\omega}_{in}^n \quad (3.31)$$

Substituting equation 3.30, and assuming $\omega_{in}^p = \omega_{in}^n$ for small angles:

$$\dot{\Psi} = -\omega_{in}^n \times \Psi + \mathbf{v} \quad (3.32)$$

3.2.3.3.2 Gyroscope Drift

Gyroscope drift was assumed to be a constant bias. There are, therefore, no dynamics associated with the drift states, which were modeled as constant states and not estimated during the covariance analysis. The drift rates were included in the initial error covariance matrix.

3.2.3.3.3 Accelerometer Errors

There are three main accelerometer error sources: accelerometer bias, scale factor, and random uncertainty. The bias errors were assumed to be the primary driving error source, the other two represent lesser effects and were not modeled.

The accelerometers measure specific force in the platform frame, which is misaligned with respect to the navigation frame by a small amount:

$$\mathbf{f}^n + \delta \mathbf{f}^n = M_p^n (\mathbf{f}^p + \delta \mathbf{f}^p)$$

which leads to:

$$\delta \mathbf{f}^n = \delta \mathbf{f}^p - \Psi \times \mathbf{f}^n \quad (3.33)$$

The misalignment vector was defined previously, and that will be crossed with the

specific force, from equation 3.26, based on the commanded speed and heading and the calculated value of gravity from equation 3.20. The accelerometer bias errors, will be modeled as Markov processes, with time constants on the order of one Martian day:

$$\dot{\delta f}^n = -\frac{1}{\tau_f} \delta f^n + q_f \quad (3.34)$$

3.2.4 The Vertical Track

The IMU vertical track is unstable, and since the navigation is assumed to be two dimensional, the second order Markov process was again used. For this case, the vertical velocity rather than the pitch was modeled:

$$\ddot{\delta h} + 2\left(\frac{2.146}{\tau_h}\right)\dot{\delta h} + \left(\frac{2.146}{\tau_h}\right)^2 \delta h = q_h$$

Substituting

$$\dot{\delta h} = \delta v_u \quad (3.35)$$

gives

$$\dot{\delta v}_u = -\frac{4.292}{\tau_h} \delta v_u - \left(\frac{2.146}{\tau_h}\right)^2 \delta h + q_h \quad (3.36)$$

3.2.5 Summary of Rover Dynamics

The rover state error equations, 3.27, 3.28, 3.29, 3.32, 3.33 can be expanded in terms of the components in the East, Up, and South directions. The vertical position and velocity error rate equations are then substituted by equations 3.35 and 3.36. For a commanded velocity, as defined in Section 3.1.1, of:

$$\mathbf{v}^n = \begin{bmatrix} v_E \\ v_U \\ v_S \end{bmatrix} = \begin{bmatrix} v \sin\gamma \\ 0 \\ -v \cos\gamma \end{bmatrix}$$

The East and South position errors are:

$$\dot{\delta r}_E = \frac{v_E}{R_m+h} \delta r_U - \frac{v_E \tan L}{R_m+h} + \delta v_E \quad (3.37)$$

$$\dot{\delta r}_S = -\frac{v_S}{R_m+h} \delta r_U + \frac{v_E \tan L}{R_m+h} + \delta v_S \quad (3.38)$$

$$\begin{aligned} \dot{\delta v}_E = & (\omega^2 - \frac{\mu}{(R_m+h)^3}) \delta r_E - (2\omega \cos L + \frac{v_E}{R_m+h}) \delta v_U \\ & - (2\omega \sin L + \frac{v_E \tan L}{R_m+h}) \delta v_S - f_S \Psi_y + f_U \Psi_z + \delta f_x \end{aligned} \quad (3.39)$$

$$\begin{aligned} \dot{\delta v}_S = & \frac{1}{2} \omega^2 \sin 2L \delta r_U + (\omega^2 \sin^2 L - \frac{\mu}{(R_m+h)^3}) \delta r_S - \frac{v_S}{R_m+h} \delta r_U \\ & + (2\omega \sin L + \frac{v_E \tan L}{R_m+h}) \delta r_E - f_S \Psi_y + f_U \Psi_z + \delta f_x \end{aligned} \quad (3.40)$$

Each of the accelerometer bias errors is modeled as a separate Markov process, with associated time constant and white noise, as shown in equation 3.34. The misalignment terms can be obtained by expanding the vector equation 3.32:

$$\dot{\Psi}_x = -(\omega \cos L + \frac{v_E}{R_m+h}) \Psi_y - (\omega \sin L + \frac{v_E \tan L}{R_m+h}) \Psi_z + v_x \quad (3.41)$$

$$\dot{\Psi}_y = (\omega \cos L + \frac{v_E}{R_m+h}) \Psi_x + \frac{v_S}{R_m+h} \Psi_z + v_y \quad (3.42)$$

$$\dot{\Psi}_z = (\omega \sin L + \frac{v_E \tan L}{R_m+h}) \Psi_x - \frac{v_S}{R_m+h} \Psi_y + v_z \quad (3.43)$$

The terms in equations 3.34 through 3.43 represent the terms in the dynamics matrix, F_R , for the IMU case. There are fifteen total states describing the rover and its IMU: three position, three velocity, three alignment, three gyro drift, and three accelerometer bias states.

For comparison with the minimal instrument case, speed and heading errors can be determined from the velocity errors. Speed is defined as:

$$v^2 = \mathbf{v}^T \mathbf{v}$$

so:

$$\delta v = \frac{1}{v} \mathbf{v}^T \delta \mathbf{v}$$

and

$$\overline{\delta v^2} = \frac{1}{v^2} \mathbf{v}^T \mathbf{E}_{vv} \mathbf{v} \quad (3.44)$$

where \mathbf{E}_{vv} is the rover velocity error covariance submatrix. The heading error, or error in the direction of the velocity vector in the horizontal plane, can be resolved from the East and South velocity components (vertical velocity is assumed zero for the nominal path):

$$\tan \gamma = -\frac{v_E}{v_S}$$

so:

$$\sec^2 \gamma \delta \gamma = -\frac{1}{v_S} \delta v_E + \frac{v_E}{v_S^2} \delta v_S$$

If a vector \mathbf{w} is defined as:

$$\mathbf{w}^T = \left[-\frac{1}{v_S}, 0, \frac{v_E}{v_S^2} \right]^T$$

Then heading error variance can be expressed in terms of the velocity error covariance submatrix:

$$\overline{\delta \gamma^2} = \cos^4 \gamma \mathbf{w}^T \mathbf{E}_{vv} \mathbf{w} \quad (3.45)$$

3.2.6 Initial Covariance Matrices

The error covariance matrix is initialized as in the minimal instrumentation case. The position errors (now East, Up, and South rather than latitude, longitude and altitude) will be correlated with the beacon errors, as before. The variances of the individual misalignments, gyroscope drift rates, and accelerometer biases are all included in the appropriate position in the matrix. Since the IMU is assumed to perform gyro compassing to align the platform with the navigation coordinate frame, the IMU errors will become highly correlated before the rover begins its journey. This gyro compassing can be simulated by performing several zero velocity updates (ZUPs) before the rover moves. These measurements provide information to the system, allowing the IMU to align the accelerometers so that only the vertical accelerometer will sense the reaction force due to gravity.

The initial white noise matrix for the IMU case has terms for only the vertical velocity channel and the three accelerometer bias channels, which are all modeled as Markov processes. The white noise values are determined as in the minimal instrument case. The vertical velocity noise is from a second order Markov process:

$$Q_h = 4 \sigma_h^2 \left(\frac{2.146}{\tau_h} \right)^3$$

and the accelerometer biases are from a first order Markov process:

$$Q_f = 2 \frac{\sigma_f^2}{\tau_f}$$

Where Q_f would be determined for each accelerometer.

3.3 Measurements

To provide more accurate estimates of the vehicle state uncertainties, measurements are taken and a Kalman filter is used to process the measurements and update the position information. For the Kalman filtering process, the measurement geometry vector and weighting factor (indicating the measurement accuracy) for each measurement are required. Two types of measurements were used in this study. The first type is radiometric range measurement taken from the orbiting satellite. Frequent range measurements were taken between the satellite and the base, and between the satellite and the rover, when in view. The other measurement was a zero velocity update (ZUP) taken when the rover stopped moving.

The two way range measurement is taken by the satellite sending a signal to the ground location, which then echoes the signal back to the satellite. The round trip time of the signal is measured and the distance between the two can be determined since the signal travels at the speed of light. As the satellite flies over, several measurements are taken, thus providing variable geometry to the measurements, giving excellent information in the vertical direction and the along track (of the satellite) direction.

The measurement geometry for the range measurement is defined in Figure 3.3. The measurement geometry vector is simply the unit line-of-site (LOS) vector between the satellite and the base or rover (in local navigation coordinates) .

$$\mathbf{u}_{los}^n = \frac{1}{\rho} \mathbf{p}^n = \frac{1}{\rho} \mathbf{M}_i^n \mathbf{p}^i = \frac{1}{\rho} \mathbf{M}_i^n (\mathbf{r}_s^i - \mathbf{r}_t^i)$$

This will give components in the navigation frame (E,U,S). For the IMU case this was what was needed. However, for the minimal instrument case, the position state was maintained as latitude, longitude and altitude. The components of the measurement geometry vector for these states is obtained through the transformation:

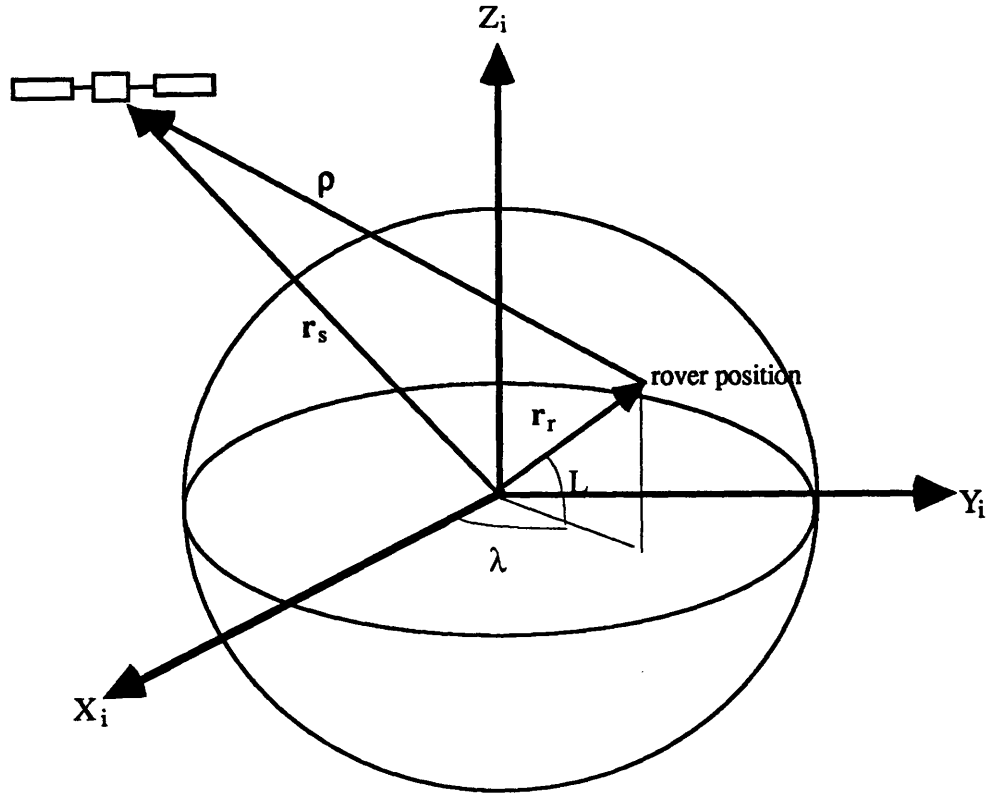


Figure 3.3: Range Measurement Geometry

$$\mathbf{u}_{\text{los}}^{\text{LLA}} = \frac{1}{\rho} \mathbf{M}_n^{\text{LLA}} \mathbf{M}_i^n \rho^i$$

The weighting factor, or measurement accuracy, is the reciprocal of the measurement error. For the range measurement, the measurement bias was modeled as a first order Markov process and included as a state in the filter to determine if the measurement error could be estimated.

$$\dot{\delta\rho} = -\frac{1}{\tau} \delta\rho + q_\rho = F_\rho \delta\rho + q_\rho$$

The time constant was chosen based on the day/night cycle of Mars causing atmospheric and temperature changes. F_p is from the dynamics matrix defined in Section 2.5.

For the ZUP, the measurement geometry vector is unity in the speed error state for the minimal instrument case, since that is all that is being measured. For the IMU, the ZUP will measure all three velocity component. For both cases, the weighting factor should be the same, and would be zero for a perfect measurement, which a ZUP quite nearly approaches. Realistically, however, a small value is needed to account for vibrations and other limiting effects. This variance for the ZUP was not estimated in the simulation, and therefore was not modeled with any dynamics.

For the IMU case, several ZUPs were taken at the beginning of the simulation. This aligned the IMU, providing an accurate measure of velocity by which the IMU could determine that the accelerations it was sensing in the East and North directions were due to gravity and caused by misalignments of the IMU.

Chapter 4: Implementation

The navigation analysis required much computation in propagating the error covariance matrix through several orbits of the satellite and updating the matrix via the Kalman filter with new information from the measurements taken. This was performed on an IBM 3090 using a HAL/S program. The program was based on existing code used for the beacon survey studies previously performed at Draper Laboratories¹⁶. The simulation uses a fourth order Runge-Kutta integration routine to propagate the satellite state, the rover state, and the error covariance matrix in time and a Kalman filtering routine, as described in Chapter 2, to incorporate the information from the measurements. Many modifications were made, most importantly adding the rover states to the filter and customizing the output for this study. Two separate simulations were developed, one for each instrument case.

Many assumptions again were made to arrive at values for many of the parameters discussed in Chapter 3. Values for the overall simulation time, satellite orbit altitude, and range measurement bias and time constant were based on the results of the beacon survey problem. The measurement error for the ZUP was chosen as a reasonably small number, providing a highly accurate, though not perfect, measurement. The values used are:

Total simulation time	50,000 sec
Satellite orbit altitude	500 km
Satellite process noise	$2.345 \times 10^{-8} \text{ m}^2/\text{s}^3$
Range measurement bias	20 m
Range measurement time constant	30,000 sec
Range measurement frequency	every 30 sec, when in view
ZUP standard deviation	0.0001 m / s

¹⁶written by Stan Shepperd, member of the technical staff, Charles Stark Draper Laboratory.

The simulation time allows several orbits of the satellite. Range measurements taken during the first two or three orbits drive down the initial position errors of the base and rover. The remaining time gives insight into the steady state error variations between satellite passes. The orbit altitude is reasonable for the assumed communications relay orbiter; it is low enough to allow for smaller omni antennas at the base and on the rover, and also provides a short period (about two hours) between flybys. The range measurement bias is representative of what is attainable with current technology and the time constant is approximately one Martian day to allow for the atmospheric changes due to heating and cooling.

4.1 Minimal Instrumentation Case

4.1.1 Baseline

A baseline of the expected, or nominal, mission profile was established, as shown in Table 4-1. These parameters were varied to determine the navigation performance sensitivity to the assumed values.

Table 4-1: Baseline Profile for Minimal Instrumentation

Satellite orbit inclination	5°
Initial Beacon Errors (East, Up, South (converted to δL_0 , $\delta \ell_0$, δh_0))	2500, 1000, 2000 meters
Initial Rover Errors (East, Up, South (converted to δL_0 , $\delta \ell_0$, δh_0))	2500, 1000, 2000 meters
Initial Beacon, Rover Position, (L, ℓ, h)	0°Lat, 0° long, 0 alt
Initial Beacon/Rover Correlation	correlated (99.99%)
Satellite range measurement	on

Zero velocity update (ZUP)	on
Rover speed, v	0.1 m / s constant
Heading, γ	45° constant
Gyro compass bias, $\delta\gamma_0$	0.5°
Gyro compass time constant, τ_γ	7200 seconds
Speedometer scale factor, σ_{sf}	0.005 (0.5%)
Speedometer time constant, τ_v	30,000 seconds
Process noise for speedometer wheel slippage, q_v	0.00001 m/s ²
Terrain model, σ_h	100 m in 1 km

To provide variable geometry range measurements and still allow constant coverage near the equator, a nominal orbit inclination of 5° was assumed. The base and rover were assumed to have landed at the equator and the initial errors in knowledge of position of the base and rover were based on reasonable knowledge attainable during landing. The errors for the rover and base were assumed to be the same and correlated for the baseline case; they are input in the navigation frame coordinates (E,U,S) and converted to latitude, longitude and altitude errors for the computation.

Range measurements are taken for both the beacon and the rover, when in view of the satellite. It is assumed that the rover stops every time the satellite comes into view: a ZUP is taken at that time (only one measurement per stop). The rover itself is assumed to travel at a constant speed of 0.1 meter per second at a constant heading of 45° (northeast). This rate is on the high side, making the nominal error case more conservative, and the heading provides insight into both latitude and longitude errors equally.

The heading error itself is assumed have a bias of 0.5°, and a time correlation of

two hours, based on previous gyrocompass models¹⁷. The Mars rotation rate is similar to the Earth's and the Schuler period is only slightly longer, 100.0 minutes compared to 84.4 minutes on Earth, so the gyrocompass is expected to function as it does on Earth. The odometer scale factor was based on a reasonable guess of the error in knowledge of wheel dimensions and contraction/expansion effects due to heating and cooling. The terrain model was determined assuming that the rover was nominally on level ground. The errors then would be how high or low the rover had actually gone. The rover was not expected to climb more than a 10° slope, thus giving an altitude error of about 10% of the distance traveled. This is a very high (conservative) estimate. The white noise value to account for wheel slippage was determined the same way, based on distance traveled, speed, and the expectation that the slipping would account for a few percent of the ultimate position error. Measurement on all wheels would help to minimize this error.

4.1.2 Simulation Trials

These baseline parameters were varied, one at a time, to determine the sensitivity of the navigation estimation to the measurements, geometry, and instrumentation accuracies. Table 4-2 shows the variations considered.

Table 4-2: Baseline Variations for Minimal Instrumentation

	<u>Baseline</u>	<u>Variational Cases</u>
Satellite orbit inclination	5°	0°, 10°
Initial Beacon Errors (East, Up, South (converted to δL_0 , $\delta \ell_0$, δh_0))	2500, 1000, 2000 meters	0, 0, 0 meters 250, 100, 200 meters
Initial Rover Errors (East, Up, South (converted to δL_0 , $\delta \ell_0$, δh_0))	2500, 1000, 2000 meters	0, 0, 0 meters 250, 100, 200 meters
Initial Beacon, Rover Position, (L, ℓ, h)	0°Lat, 0° long, 0 alt (m)	10°, 45°, 70° latitude

¹⁷Kriegsman, B. et al, "Deep Ocean Mine Site Navigation System Evaluation Final Report", Draper Laboratory, R-1049, January 1977, pp 22-26.

Initial Beacon/Rover Correlation	correlated (99.99%)	uncorrelated
Satellite range measurement	on	off
Zero velocity update (ZUP)	on	off
Rover speed, v	0.1 m / s constant	0.05, 0.5, 1.0 m / s constant and slight sinusoidal
Heading, γ	45°	0°, 90°, circle (varying)
Gyro compass bias, $\delta\gamma_0$	0.5°	0.1°, 1°, 2°
Gyro compass time constant, τ_γ	7200 seconds	
Speedometer scale factor, σ_{sf}	0.005 (0.5%)	0.001, 0.01, 0.05, 0.1
Speedometer time constant, τ_v	30,000 seconds	
White noise for speedometer wheel slippage, q_v	0.00001 m/s ²	
Terrain model σ_h	100 m in 1 km	100 m in 10 km

4.2 IMU Case

4.2.1 Baseline

The baseline for the IMU case is shown in Table 4-3. The satellite orbit, initial position errors, and measurement values are from the minimal instrument case. The IMU error values were based on available instruments of modest quality. The parameters were varied to determine how the navigation accuracies are affected.

Table 4-3: Baseline Profile for the IMU

Satellite orbit inclination	5°
Initial Beacon Errors (East, Up, South)	2500, 1000, 2000 meters
Initial Rover Errors (East, Up, South)	2500, 1000, 2000 meters
Initial Beacon, Rover Position	0°Lat, 0° Long, 0 Alt (m)
Initial Beacon/Rover Correlation	correlated (99.99%)
Satellite range measurement	on
Zero velocity update (ZUP)	on
Terrain model	100 m in 1 km
IMU gyro drift	0.02 deg/hr
IMU initial misalignment	60 arcsec
IMU accelerometer bias	50 μ g

4.2.2 Simulation Trials

Table 4-4 shows the variations of the IMU errors considered. The other variables were varied as in the minimal instrument case.

Table 4-4: Baseline Variations for the IMU

	<u>Baseline</u>	<u>Variational Cases</u>
Satellite orbit inclination	5°	0°, 10°
Initial Beacon Errors (East, Up, South)	2500, 1000, 2000 meters	0, 0, 0 meters 250, 100, 200 meters
Initial Rover Errors (East, Up, South)	2500, 1000, 2000 meters	0, 0, 0 meters 250, 100, 200 meters
Initial Beacon, Rover Position	0°Lat, 0° Long, 0 Alt (m)	10°, 45°, 70°
Initial Beacon/Rover Correlation	correlated (99.99%)	uncorrelated
Satellite range measurement	on	off

Zero velocity update (ZUP)	on	off
Terrain model	100 m in 1 km	100 m in 10 km
IMU gyro drift	0.02 deg/hr	0.05, 0.5, 0.1, 1 degree/hr
IMU initial misalignment	60 arcsec	100 arcsec
IMU accelerometer bias	50 μ g	100 μ g, 500 μ g

Chapter 5: Results

5.1 Minimal Instrumentation

The rover position errors relative to the base site are plotted in Figures 5.1 through 5.3 for the baseline case (Gyrocompass and speedometer). Figure 1 shows the errors in the East/West direction, starting from an initial relative error of 35 meters. This assumed that both the beacon and rover absolute initial errors in the East direction were 2500 meters and that the errors were highly correlated (99.99%). Actually, the initial correlation would probably produce a smaller initial relative error than was modeled, but the ultimate steady state errors would not be affected.

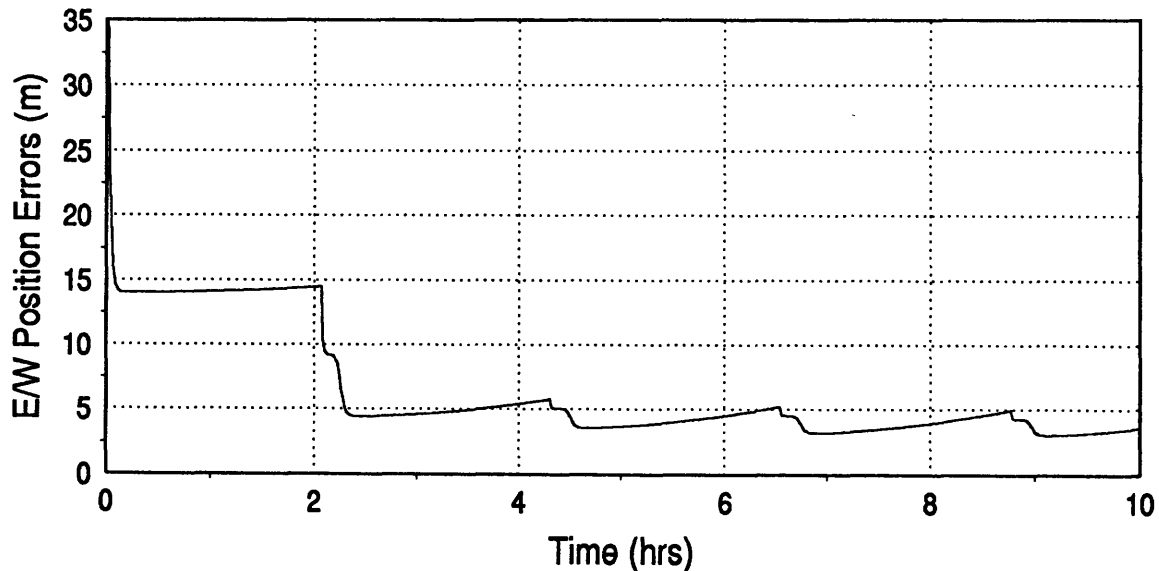


Figure 5.1: Baseline Minimal Instrumentation Relative E/W Position Errors

The figure shows that the initial satellite range measurements taken at the beginning of the simulation, reduces the error considerably. A steady state is reached after the third satellite pass, showing that the speedometer and gyrocompass allow the East/West position errors to grow only two meters between satellite passes. When the satellite is in view, the rover stops and a ZUP is taken, then range measurements are taken

every minute while the satellite is in view. These measurements drive the rover relative position errors back down to just three meters.

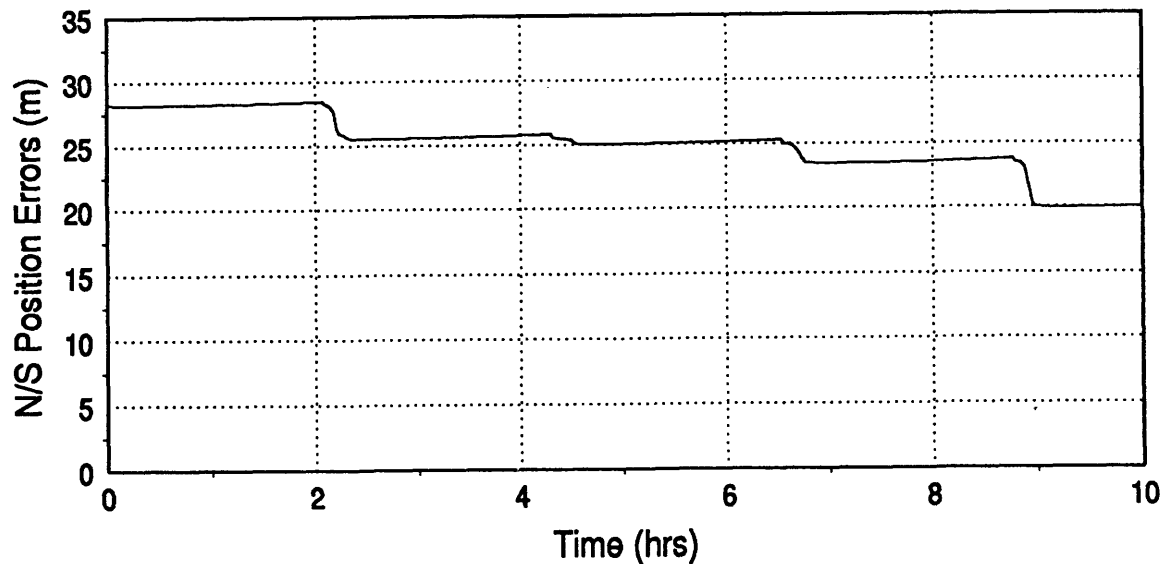


Figure 5.2: Baseline Minimal Instrumentation Relative N/S Position Errors

The rover relative position errors in the North/South direction are shown in Figure 5.2. Again, the initial relative error of 28 meters is conservative due to the modeling of the initial rover-base position error correlations. The range measurements do not provide as accurate a measurement, since the rover is assumed to be on the equator and the satellite is in only a 5° inclination orbit. The North/South observability is limited since the relative geometry between the two does not provide as much information initially as in the East/West case. It is clear that with each successive satellite pass the geometry varies more as the satellite ground track shifts, resulting in more accurate range measurements. The error growth between passes is not as great as in the East/West case since the actual errors in position are not being driven down as much by the range measurements, so the in the root mean squared error growth due to the onboard instruments is small compared to the initial errors after each satellite pass. Although not shown, the steady state errors are reached after eight satellite passes, at a value of 15 meters.

Though the rover navigation problem is fundamentally two dimensional, Figure

5.3, showing the relative rover vertical errors, is included to show the results of the vertical track error modeling, which did contribute to the errors in the other two directions.

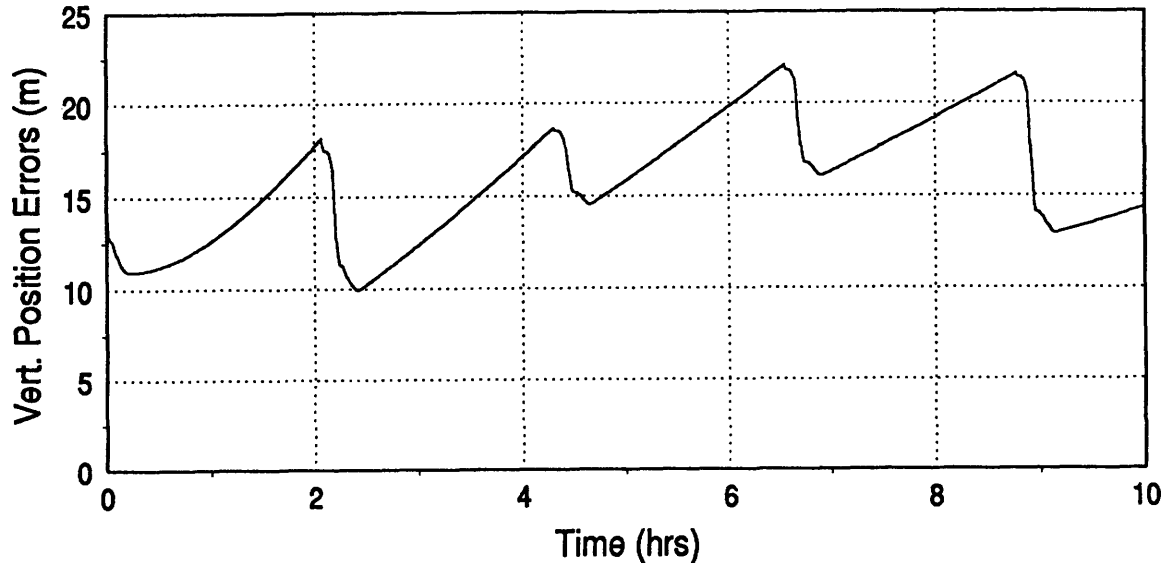


Figure 5.3: Baseline Minimal Instrumentation Relative Vertical Position Errors

The range measurements clearly drive down the relative vertical errors. If the altitude error growth of the rover was not modeled, the relative errors would be constant between the satellite passes. Relative error growth of five meters in the vertical track is reasonable for a vehicle traveling approximately 720 meters (0.1 meters per second for approximately two hours).

The speed and heading errors were also plotted for the baseline case. Figure 5.4 shows the growth in speed errors between stops. The ZUP taken as the rover stops when the satellite comes into view, drives down the velocity error to the value of the ZUP measurement error. When the rover starts to move again, the speed errors grow until the next measurement. The growth is indicative of the Markov process driving the scale factor, though it is steeper due to the extra white noise which was added to model the wheel slippage. The magnitude of the speed error is small, but the rover is only traveling at 0.1 meter per second so the speed error was only expected to be a small percentage of that, due to slippage and expansion/contraction of the wheel used to count rotations.

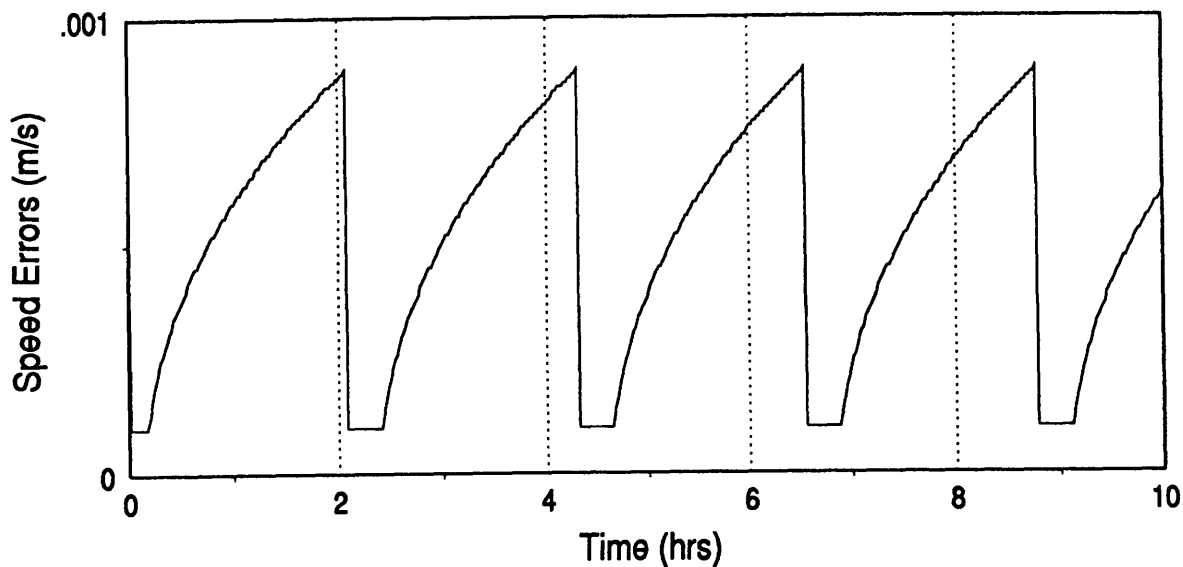


Figure 5.4: Baseline Minimal Instrumentation Speed Errors

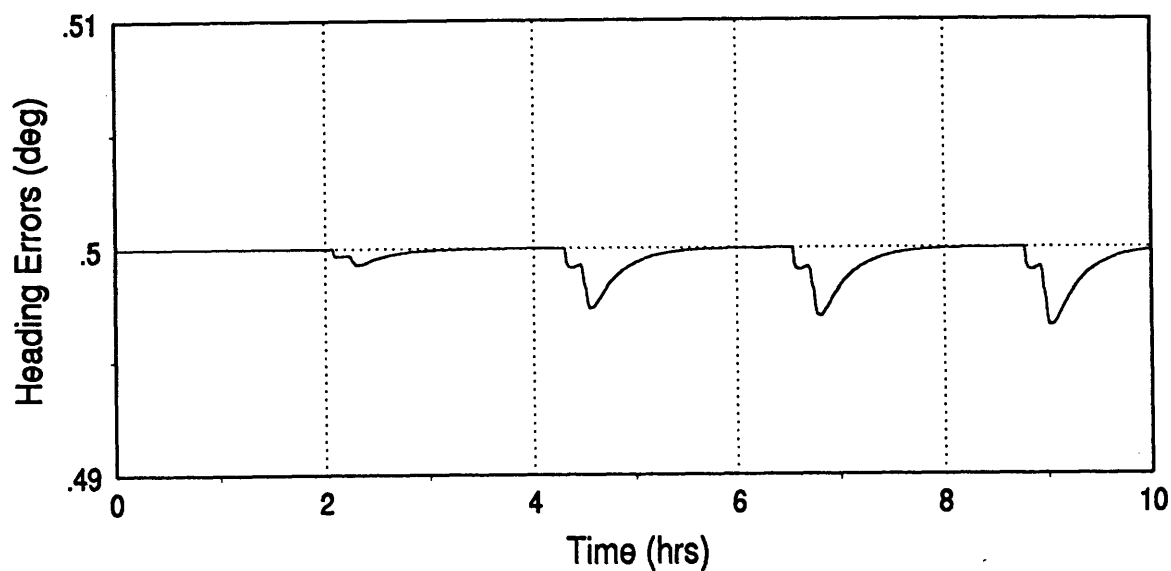


Figure 5.5: Baseline Minimal Instrumentation Heading Error

The heading error, shown in Figure 5.5, remained close to its nominal 0.5° error (note the range of the scale of the figure). When the range measurements were taken and the rover position errors estimated, the error in the heading could also be estimated better. With each satellite pass, the rover position was determined with more accuracy, thus the heading error was reduced slightly more each time, but quickly drove back up to the 0.5° bias. The heading error was basically not estimable with the frequency of measurements

being taken, though, as was shown, a 0.5° heading error did not cause a problem with the growth of the position errors between measurements.

Assuming that there were no initial errors in position but the instruments provided the baseline error contributions, the effects of the instrument errors can be seen. Figure 5.6 and 5.7 show the East/West and North/South absolute rover position errors, respectively, assuming that the initial rover position was known exactly. The three curves on each graph indicate the open loop performance of the instruments, the performance if only ZUPs are taken, and the performance if only range measurements are taken.

The open loop growth is almost linear, with errors in both directions reaching 30 meters after ten hours with the rover traveling at a heading of 45° . The ZUPS actual show better performance than the range measurements in this case, but that is due to the fact that the range measurement bias is twenty meters and the actual rover errors are very small initially. The ZUPs are very accurate and effective at keeping down the actual rover errors if they are initially small. The East/West and North/South error propagation is identical, except for the case of the range measurements, which is due to the relative geometry of the satellite and rover.

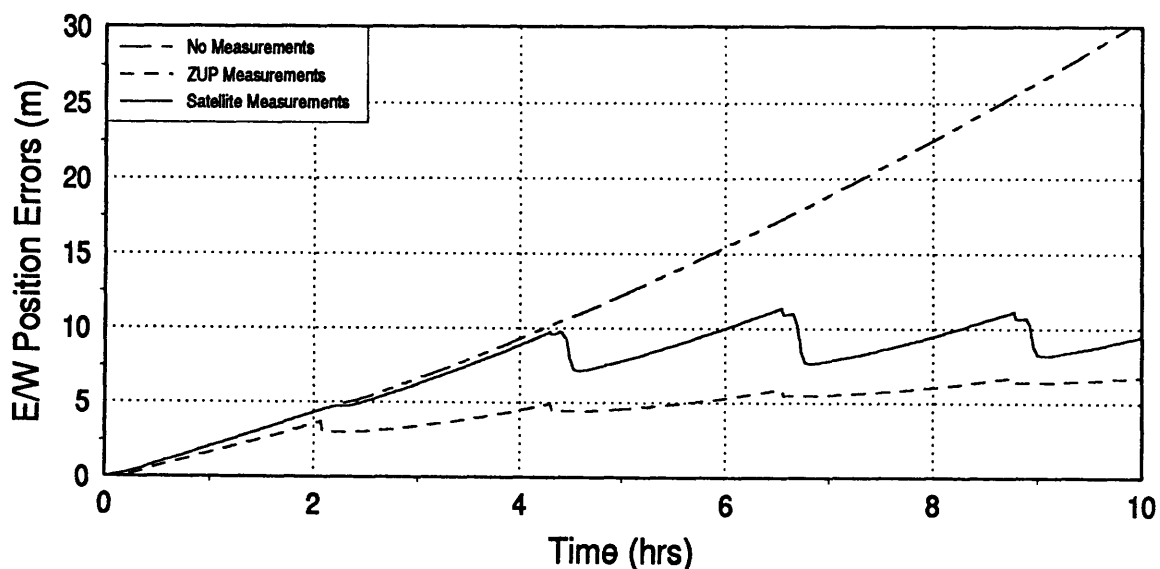


Figure 5.6: Minimal Instrument Rover E/W Position Error Growth
(Assuming Zero Initial Errors)

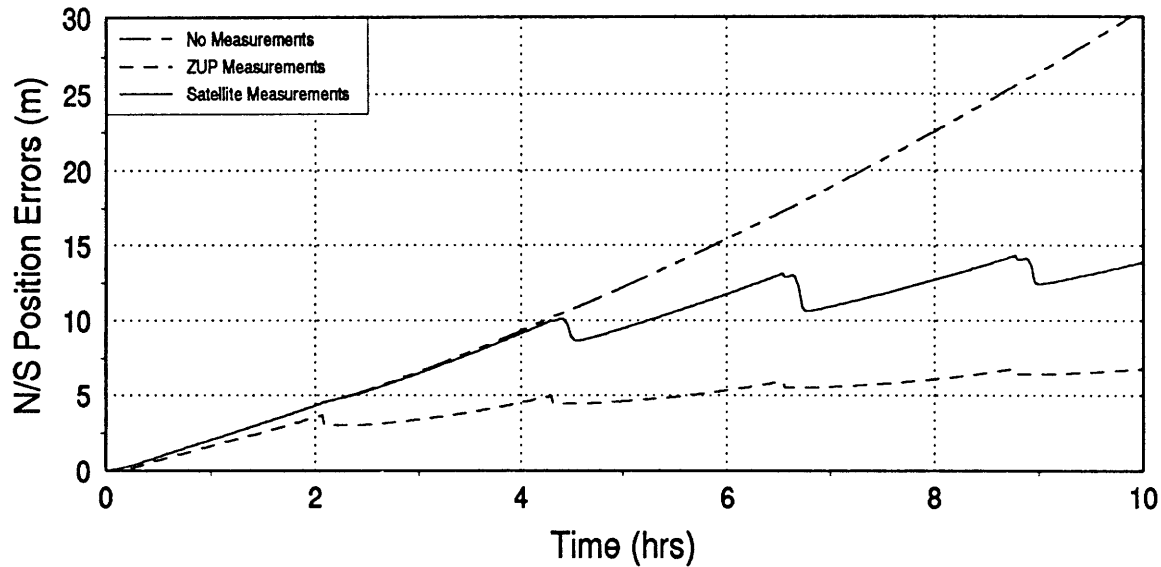


Figure 5.7: Minimal Instrument Rover N/S Position Error Growth
(Assuming Zero Initial Errors)

A comparison of ZUPs and satellite range measurements was also made for the baseline case, as shown in Figures 5.8 and 5.9. Using ZUPs alone did not reduce the relative errors in the rover position from their initial correlated value, but also did not allow the errors to grow beyond these values between satellite passes. The range measurements were, again, much more effective in the East/West direction (Figure 5.8) than in the North/South (Figure 5.9).

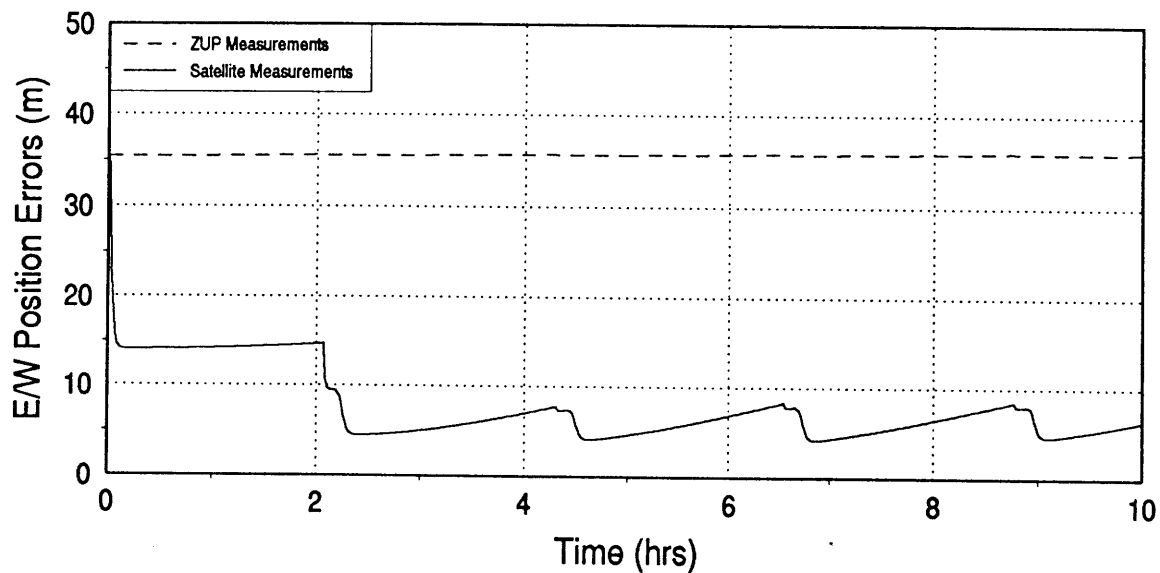


Figure 5.8: Minimal Instrument E/W Errors for ZUPS vs Range Measurements

With only the range measurements, the steady state relative errors in the East/West direction are about twice that of the baseline case, with both measurement types, indicating that the ZUPS play an important role in reducing the errors when used with range measurements. This is even more evident in Figure 5.9 for the North/South errors, where the error growth between satellite passes drives up the rover relative position errors, keeping them close to their initial conditions. With both measurements, the North/South position errors are consistently reduced over the first few satellite passes, as shown in Figure 5.2

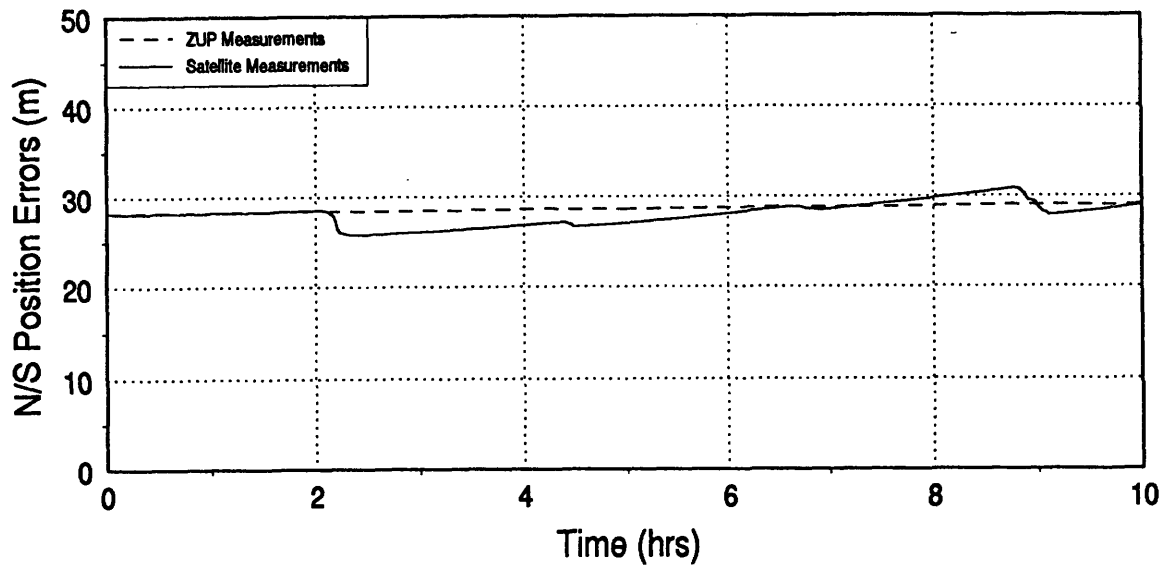


Figure 5.9: Minimal Instrument N/S Errors for ZUPS vs Range Measurements

The variations in the parameters from the baseline had little effect in general. As expected, varying the inclination of the orbit affected the North/South errors most significantly, changing the East/West steady state relative errors by less than half of a meter. For a 0° inclination orbit, the North/South errors remained at their initial value, as if no range measurements had been taken. The satellite/rover geometry provided no information across the path of the satellite. The ZUPs only curve in Figure 5.8 is indicative of the response for this case. A 10° inclination orbit provided more variance in the relative measurement geometry for the North/South error estimation, reaching a steady state of about a 10 meter error compared with the 15 meter error of the baseline

case. The East/West errors increased slightly (by less the half a meter).

If the base and rover position errors were initially assumed to be uncorrelated, the same steady state relative errors were achieved, though after two additional satellite passes. The base errors and rover errors became highly correlated as a result of the range measurements and their close proximity. Reducing the altitude bias had no significant affect on the errors in the horizontal plane, though it did reduce the steady state relative vertical error by about a meter.

Placing the rover/base at a different latitude did affect the error results. At 10° latitude, the both the East/West and North/South errors increased by less than a meter, though the vertical errors increased by almost 10 meters, due to the geometry of the range measurement. At 45° latitude, however, the degradation in the estimation of relative position was substantial. At that latitude, the satellite was never in view of the base or rover, so only ZUPS were taken. The errors in the East/West direction grew to over 65 meters after ten hours, compared to the 35 meter steady state for the equatorial location, as seen in Figure 5.8. The North/South errors increased to over 45 meters compared to the steady state of 30 meters seen in Figure 5.9. At 70° latitude the East/West errors increased more significantly, reaching over 110 meters after 10 hours; the North/South errors grew at the same rate as at 45° latitude. Obviously, the model used breaks down at higher latitudes, as mentioned before.

Varying the speed and heading of the rover were also addressed. The heading of the rover had little affect on the ultimate relative error estimates. For the short distances traveled, the range measurement geometry varied only slightly, so the results of the range measurements were not significantly changed. The errors were more sensitive to the rover speed, however. Table 5-1 shows the effects of speed on the errors. Reducing the speed shows little advantage, but significantly increasing the speed reduces the speedometer performance considerably. Since the distance traveled is greater between satellite passes, the effect of the heading error on position is also more significant. It is

not expected, however, that a small unmanned rover will travel at speeds in excess of 0.1 meter per second, so this sensitivity should not present a problem to the use of the speedometer and gyrocompass for semi-autonomous navigation.

Table 5-1: The Effect of Rover Speed on Relative Position Errors

	East/West Relative Errors	North/South Relative Errors
0.05 m/s	3 - 4 m	12 - 14 m
Baseline, 0.1 m/s	3 - 5 m	14 - 16 m
0.5 m/s	4 - 15 m	26 - 30 m
1.0 m/s	5 - 30 m	30 - 45 m

The relative position errors were not sensitive to the instrument errors. Tripling the speedometer scale factor had no effect on the North/South errors and only increased the East/West errors by less than half a meter. Increasing the scale factor by ten times, making the error of the speedometer 5% of the speed traveled, increased the East/West errors by only one meter and the North/South errors by less than three meters. Reducing the scale factor by a fifth was equally ineffective in reducing the position errors as increasing the scale factor was in increasing the position errors. Almost identical results were seen in the cases where the gyrocompass bias was increased and decreased; the maximum bias considered was 2° , four times the baseline value, and the errors in both directions were increased by less than one meter.

Finally, reducing the initial position errors of the rover and base was considered. If the location of a landing craft was surveyed using the star tracker measurements to supplant the range measurements, which was the topic of previous studies at Draper as discussed in Chapter 2¹⁸, the actual initial location of the rover would be known fairly

¹⁸T.J. Brand and S.W. Shepperd, "Candidate Mars Local Navigation Infrastructures", AAS 91-496, AAS/AIAA Astrodynamics Specialist Conference, August 19, 1991.

accurately. By using initial position errors which were 10% of the baseline, the initial correlated relative errors were also lower. This resulted in an ultimate reduction of the relative position errors in the North/South direction to 6 meters from 15 meters. The steady state errors in the other tracks were not affected by reducing the initial position errors, though the steady state was reached more quickly. This reduction in the North/South errors can largely be attributed to the lower initial relative errors. This could also be achieved through higher correlation of the initial base/rover position errors.

5.2 Full IMU Case

It was initially expected that the navigation performance provided by the IMU would exceed that of the speedometer and gyrocompass; the contrary resulted. Figures 5.10 and 5.11 show the baseline East/West and North/South relative position errors, respectively, using a modest IMU as described for the baseline case. Several ZUPs were performed initially to align the IMU, and, as with the minimal instrument case, the rover stopped when the satellite came into view and a ZUP was taken. Range measurements were taken every minute while the satellite remained in view of the rover.

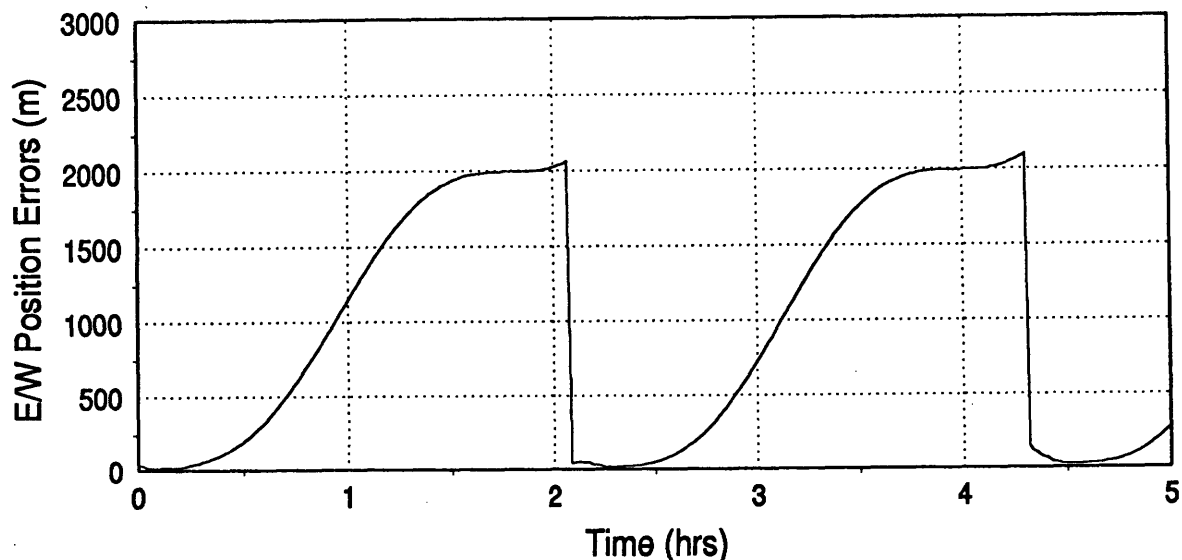


Figure 5.10: Baseline IMU E/W Relative Position Errors

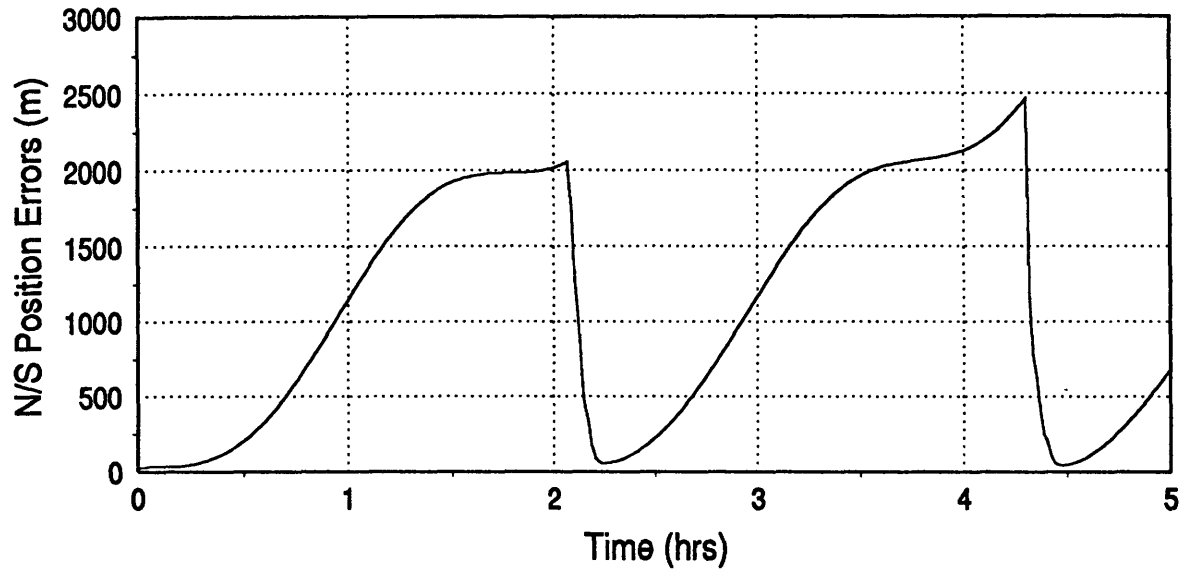


Figure 5.11: Baseline IMU N/S Relative Position Errors

Both figures show the problems of using accelerometers to determine translational motion in a gravity environment. The drops in the curves indicate when the range and ZUP measurements are taken. The relatively gradual initial rise, compared with the two subsequent rises, is due to the ZUP measurements used to initially align the IMU. Though an IMU can be aligned initially with high accuracy, even a small misalignment and subsequent drift can cause large errors in accelerometer readings. The horizontal accelerometers are detecting specific forces due to gravity which are erroneously integrated to determine velocity and position. A 60 arcsec horizontal misalignment of the platform is the equivalent of about a 100 μg bias error in the accelerometer on Mars.

Speed and heading errors were also plotted for the IMU case, determined from equations 3.39 and 3.40. Both were determined from the errors in the three components of the velocity. The speed error, shown in Figure 5.12, varies from 0.1 to 0.6 meters per second, which is greater than the speed itself. Again, this is due to the accelerometers sensing the reaction forces due to gravity. The drops to zero error indicate when the rover stops and ZUPS are taken; the speed errors are undefined when the rover stops. The ZUPs do reduce the speed errors, which can be noted by the starting point of the errors after the rover starts again.

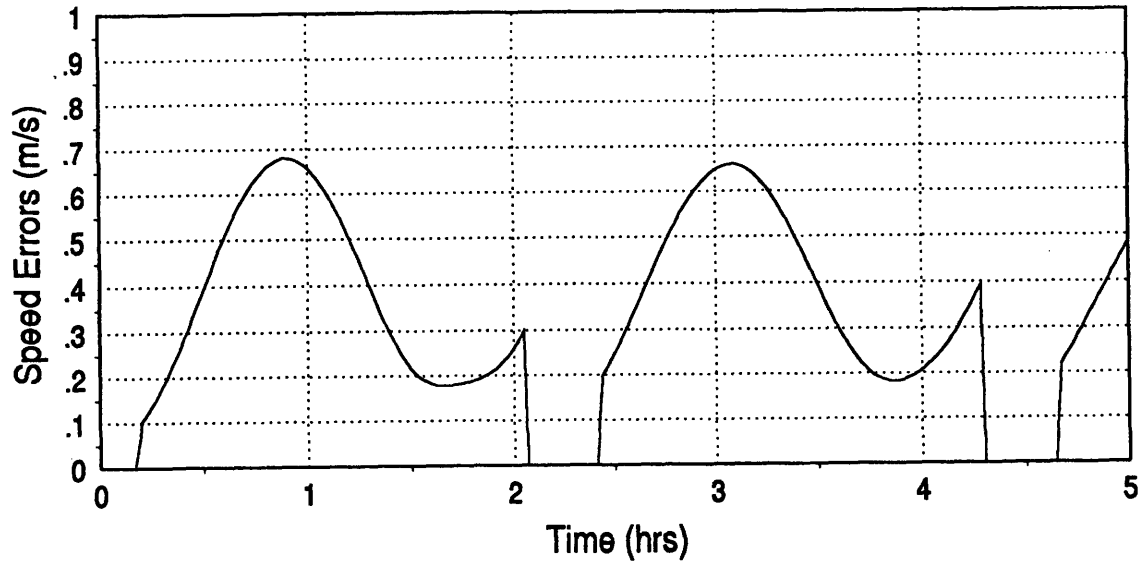


Figure 5.12: Baseline IMU Speed Errors

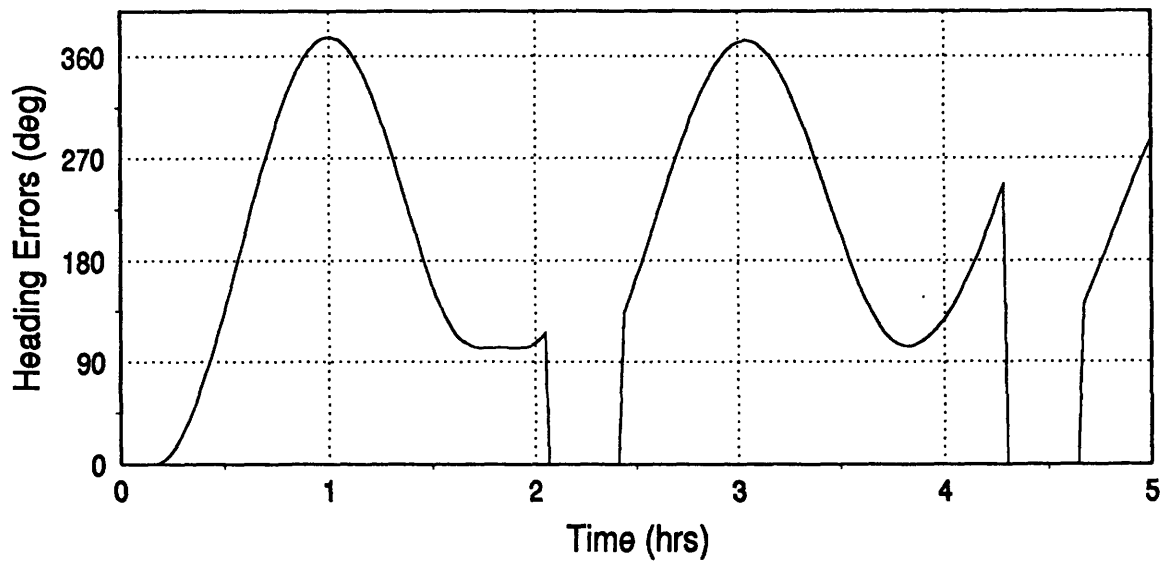


Figure 5.13: Baseline IMU Heading (Velocity Direction) Errors

Figure 5.13 shows the heading errors, which are actually the errors in the determination of the direction of the velocity vector as calculated in equation 3.40. Since the speed error is greater than the speed itself, the error in knowledge of the direction of the velocity vector is enormous. The actual heading of the rover can be obtained from the attitude information maintained by the gyroscopes. If the gyroscopes initially align the platform with the navigation coordinate frame, then the error in the rover attitude is based

on the initial small misalignment (baseline 60 arcsec) and drift rate (baseline 0.02 arcsec/sec), propagated as shown in equation 3.43. This will be very small, for the baseline gyroscope.

For further comparison with the speedometer and gyrocompass, results were plotted assuming perfect knowledge of the rover initial position to see the open loop performance of the instrument errors. As with all of the figures for the IMU case, these show oscillatory error results. This is indicative of the natural response of an inertial measurement unit in a gravity environment¹⁹. Figures 5.13 and 5.14 show the errors in the East/West and North/South directions, respectively. Both figures are similar for the case where no measurements are taken. The ZUPs reduce the errors slightly, and keep them in check, as can be seen by the last ZUP taken at just over four hours, but do not have a significant overall effect on the accuracy. The range measurement provided much more accuracy for the East/West errors, similar to that seen in the baseline case, bounding the errors to about 2000 meters and bringing them down to just a few meters when the measurements were taken.

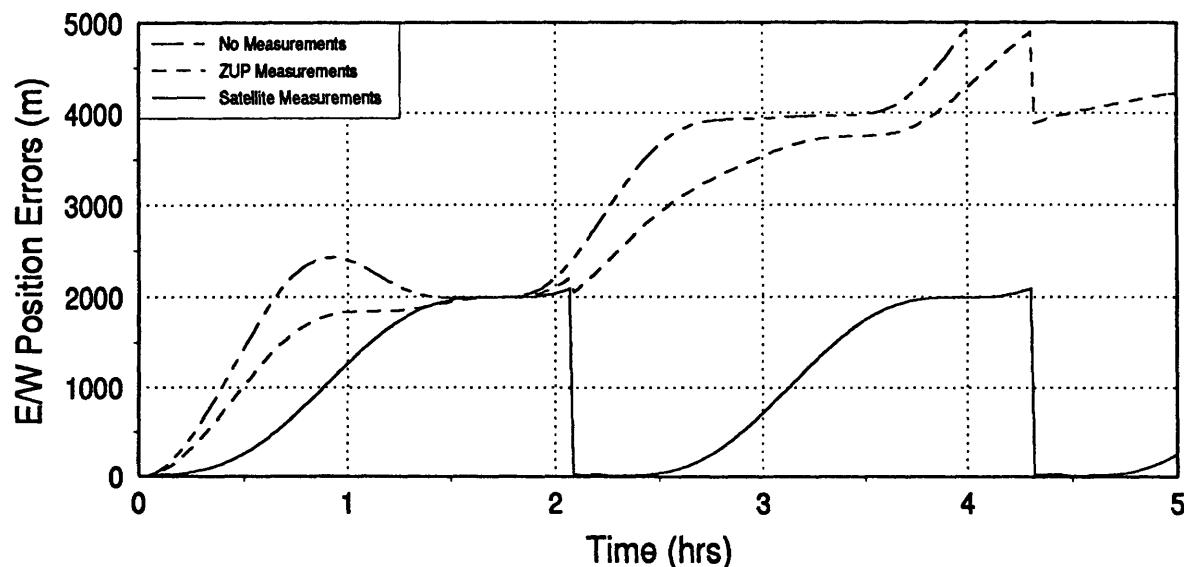


Figure 5.14: IMU Rover E/W Position Error Growth
(Assuming Zero Initial Errors)

¹⁹K.R. Britting, "Inertial Navigation Systems Analysis", Wiley-Interscience- a Division of John Wiley & Sons, Inc., New York, NY, 1971, pp 128-152.

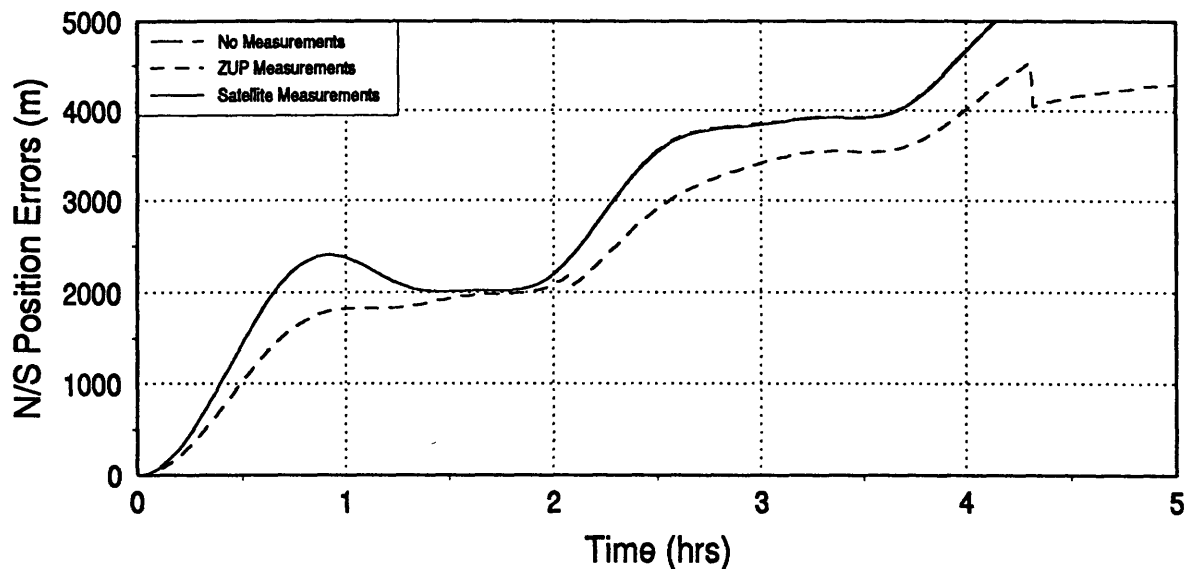


Figure 5.15: IMU Rover N/S Position Error Growth
(Assuming Zero Initial Errors)

The North/South errors were not affected by the range measurements since the satellite in this test case was at 0° inclination and the rover was on the equator, providing no measurement geometry for the North/South direction. If the satellite inclination was at 5° , the results would match the baseline case, as with the East/West errors.

The effect of ZUPs and range measurements were also considered for the relative rover errors in the baseline case. The East/West relative error are significantly reduced by the range measurements compared to the ZUPs, as shown in Figure 5.16. This is similar to the growth seen in Figure 5.14, since the initial relative errors are on the order of a few meters and the rover actual position errors grow significantly after the first range measurements are completed. The North/South position errors shown in Figure 5.17 have a similar response to the ZUPs, being reduced initially by the alignments. When only satellite measurements are taken, the initial relative errors grow quickly since the first range measurements are taken with the satellite directly overhead and the measurements cannot provide a good estimate of the actual rover (or base) errors in the North/South directions. Subsequent satellite passes provide better measurement

geometry, allowing a better estimate of the North/South errors. The ZUPs are clearly much more significant to keeping the North/South errors down than the East/West errors, which can be seen by comparing Figures 5.16 and 5.17 with Figures 5.10 and 5.11.

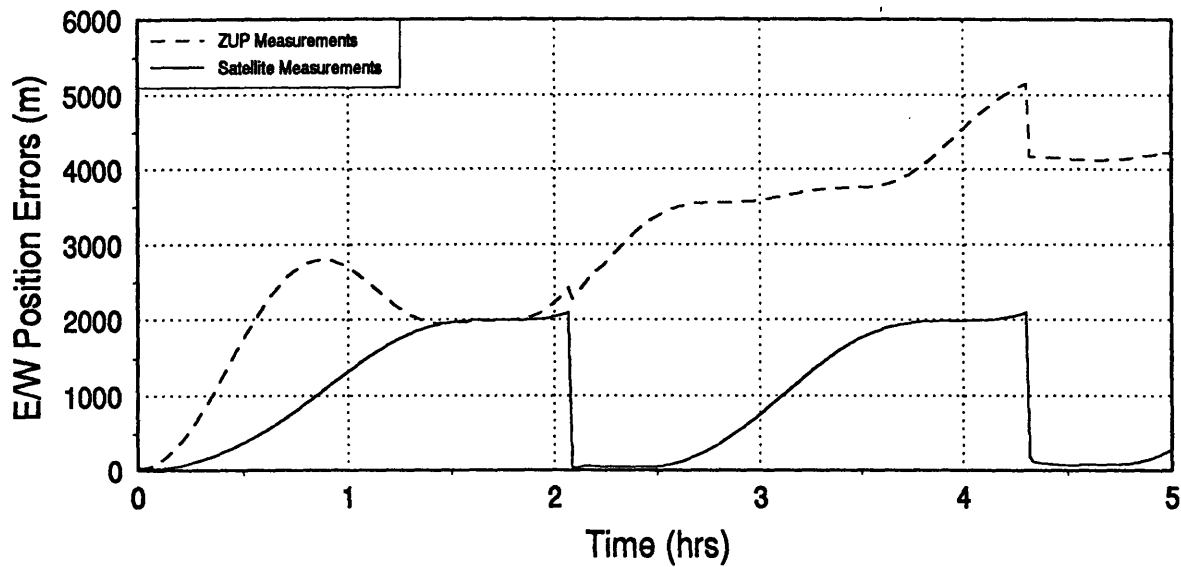


Figure 5.16: Baseline IMU E/W Errors for ZUPS vs Range Measurements

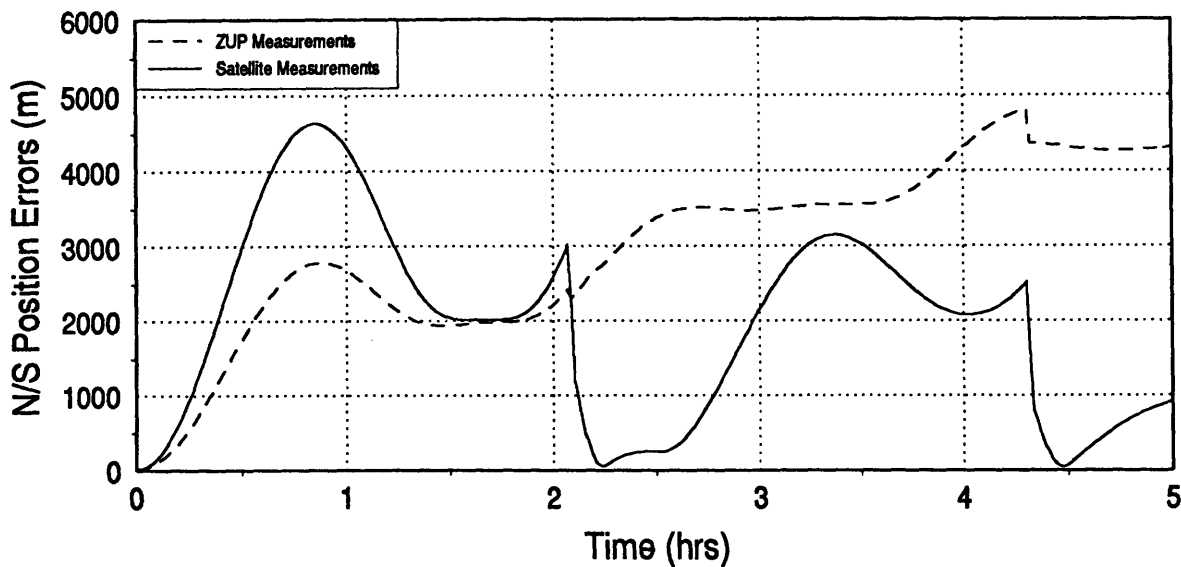


Figure 5.17: Baseline IMU N/S Errors for ZUPS vs Range Measurements

Since the navigation performance of the IMU baseline was not nearly as good as the speedometer and gyrocompass, further study of the IMU was not pursued. For the

IMU to be effective, it requires external measurements to maintain alignment and calibration of the accelerometers. Frequent ZUPs could be taken, if the rover was commanded to stop regularly, but the number required would seem prohibitive given the overall effectiveness of single ZUP measurements. Using a speedometer or odometer in conjunction with an IMU could also provide an external measurement to correct the accelerometer errors, but this makes an even more costly instrument package.

The initial alignment of the IMU could be accomplished by other means than ZUPS, which could provide a better initial alignment of the IMU and thus better navigation accuracy for the rover. The basic nature of the response would remain the same, though the open loop growth would not be as great as seen in the cases studied. The IMU error growth still would be unbounded, however, and the instrument still would require more frequent external measurements than those provided by the satellite to maintain its alignment. The open loop position growth between satellite passes would still greatly exceed that of the minimal instrument case.

Chapter 6: Conclusions

The results of this feasibility study indicate that simple instruments, specifically a speedometer and gyrocompass, provide very good semi-autonomous navigation performance, especially in the East/West direction. A satellite in a low inclination orbit provides the vital range measurements to maintain the relative position accuracy, but the onboard instruments allow only slight error growth between passes. The models used for the onboard instruments were simple, but the ultimate relative rover position errors were insensitive to the accuracies of these instruments, indicating that any reasonable indication of speed and heading provides adequate information to navigate open loop for short periods between a low orbiting satellite pass. The effectiveness of the gyrocompass is inhibited at high latitudes, as discussed in Section 2.1.

Due to the combined effect of accelerometer misalignment and gravity, the IMU, by itself, was deemed inadequate to provide the open loop navigation between satellite passes for a slow moving rover. Though an IMU could be useful if additional external measurements were regularly provided (from a speedometer for instance) the accuracy of this complicated system would not substantially improve that of the minimal instrument case, which is less costly and less complicated. Adding a speedometer would, in effect, simply replace the gyrocompass in the minimal instrument case with an IMU. Greater accuracy in heading could be achieved, but the study determined that the ultimate position accuracy was not significantly affected by heading accuracy.

It is interesting to note that the relative navigation problem can be accomplished without knowing the actual base or rover positions in an inertial sense. Though it was shown that an initial survey of the base/rover position was not required to provide accurate relative navigation performance, an initial survey of the base site relative to surface features would be required. An optical survey presumably would provide the best information of the terrain to be explored by the rover and it is assumed such a survey was

conducted prior to the rover mission. The location of the landing craft and rover relative to surface features could be determined through a map-tie of images taken by the landing craft during descent and the images from the initial survey. A course to avoid hazards and obstacles could then be planned for the rover. Further study of this terrain survey problem should be pursued in tandem with the navigation problem presented in this thesis.

Once specific rover missions are determined, more accurate models can be derived for the instrumentation and the specific accuracy requirements for the mission can be verified.

Bibliography

- Augustine, N., et. al., "Report of the Advisory Committee on the Future of the US Space Program", NASA, PB91-181529, December 17, 1990.
- Battin, R.H., "An Introduction to the Mathematics and Methods of Astrodynamics", AIAA Press, New York, NY, 1987, pp 627-632.
- Benson, Jr., D.O., "A Comparison of Two Approaches to Pure-Inertial and Doppler-Inertial Error Analysis", IEEE Transactions on Aerospace and Electronic Systems, Vol AES-11, No. 4, July 1975.
- Brand, T.J., and S.W. Shepperd, "Candidate Mars Local Navigation Infrastructures", AAS 91-496, AAS/AIAA Astrodynamics Specialist Conference, August 19, 1991.
- Breckenridge, W.G., and T.C. Duxbury, "Spacecraft-Based Navigation System", Aeronautics and Astronautics, Vol 8, No 5, May 1990.
- Britting, K.R., "Inertial Navigation Systems Analysis", Wiley-Interscience, a Division of John Wiley & Sons, Inc., New York, NY, 1971, pp 86-88.
- Cohen, A. "The Report of the 90-Day Study of Human Exploration of the Moon and Mars", NASA, November 1989.
- Gamble, J.D., "JSC Pre-Phase Study, Mars Rover Sample Return Mission, Aerocapture, Entry, and Landing Element", JSC-23230, NASA, Johnson Space Center, May 1989.
- Gelb, A., Editor, "Applied Optimal Estimation", The MIT Press, Cambridge, MA, 1974, pp 27-34.
- Heller, W.G., "Free-Inertial and Damped-Inertial Navigation Mechanization and Error Equations", TASC No. TR-312-1-1, The Analytical Sciences Corporation, Reading, MA, April 18, 1975.
- Kriegsman, B. et al, "Deep Ocean Mine Site Navigation System Evaluation Final Report", Draper Laboratory, R-1049, January 1977, pp 22-26.
- Mutch, T.A., et.al., "The Geology of Mars", Princeton University Press, Princeton, NJ, 1976, pp 29-30.
- Pivrotto, D.S. and W.C. Dias, "United States Planetary Rover Status - 1989", NASA/JPL, JPL Publication 90-6, May 15, 1990.
- Spratlin, K.M., et.al., "1989 Lunar/Mars Initiative Guidance, Navigation & Control Final Report", CSDL-P-2932, The Charles Stark Draper Laboratory, Inc., Cambridge, MA, February, 1990.
- Sturms, F., et.al., "Concept for a Small Mars Sample Return Mission Using Microtechnology", NASA/JPL, JPL Publication D-8822, October 1991.
- Wrigley, W., W.A. Hollister, and W.G. Denhard, "Gyroscopic Theory, Design and Instrumentation", The MIT Press, Cambridge, MA, 1969, pp 187-209.

Appendix A: Notation

Scalars	lower case letters, angles are usually represented as Greek symbols
Vectors	lower case, bold letter (\mathbf{r}), if superscripted, the superscript represents the coordinate frame the vector is taken in (\mathbf{r}^i - is in inertial coordinates)
Matrices	upper case, bold letter (\mathbf{M})
Transformation Matrices	upper case, bold \mathbf{M} with indices to show coordinate systems involved. Subscript index is 'from' frame, superscript is 'to' frame (\mathbf{M}_n^i is a transformation from the navigation frame to inertial coordinates).
Time derivatives	first derivative is a single dot ($\dot{}$) over the variable, second derivative is a double dot ($\ddot{}$) over the variable
Perturbation (error) quantities	variable being perturbed is preceded by a (δ) symbol
Measured quantities	variable (scalar or vector) with a (\sim) over top, ($\tilde{\mathbf{r}}$)
Estimated quantities	variable (scalar or vector) with a (\wedge) over top, ($\hat{\mathbf{r}}$)

Appendix B: Variable Definitions

$\{X_i, Y_i, Z_i\}$	Inertial coordinate frame (i)
$\{E, U, S\}$	Navigation coordinate frame (n) - (East, Up, South)
$\{x_p, y_p, z_p\}$	platform frame (p)
$\{x_e, y_e, z_e\}$	planet-fixed, planet-centered frame (e)
α	pitch of rover
B	matrix of measurement geometry vectors
β	roll of rover
b	geometry measurement vector
E	error covariance matrix
ϵ	error in estimation of the deviation from the nominal trajectory
E_B	error covariance matrix for the home base states
E_R	error covariance matrix for the rover states
E_{RR}	error covariance matrix for the rover position states
E_{VV}	error covariance matrix for the rover velocity states
E_S	error covariance matrix for the satellite states
F	dynamics matrix (subscript represents portion of full matrix)
f	specific force (sensed acceleration) vector
$\Phi(t, t_0)$	state transition matrix
F_B	dynamics matrix for the home base states
F_R	dynamics matrix for the rover states
F_p	dynamics term for the range measurement state
F_S	dynamics matrix for the satellite states

\mathbf{G}	gravity gradient matrix
\mathbf{g}	gravitation vector
g	gravity magnitude
\mathbf{g}	gravity vector
γ	heading
h	altitude from planet surface
L	latitude
λ	celestial longitude
ℓ	longitude
μ	Mars gravitation constant
\mathbf{M}_m^i	transformation matrix from Mars fixed frame to inertial
\mathbf{M}_n^i	transformation matrix from the navigation frame to inertial
\mathbf{M}_n^{LLA}	transformation matrix from navigation to lat, long, alt
\mathbf{M}_n^m	transformation matrix from navigation frame to Mars fixed
\mathbf{Q}	covariance noise matrix
\mathbf{Q}_α	variance of noise in vertical channel of rover movement
q_α	white noise driving pitch uncertainty
\mathbf{Q}_B	covariance noise matrix for the home base states
q_f	white noise driving accelerometer bias model
q_γ	white noise driving gyrocompass error
q_h	white noise driving altitude bias, in IMU case
\mathbf{Q}_R	covariance noise matrix for the rover states
\mathbf{Q}_s	covariance noise matrix for the satellite states
\mathbf{Q}_s	variance of noise due to wheel slippage for speedometer
q_s	white noise driving wheel slippage model

Q_v	variance of speedometer scale factor noise
q_v	white noise due to speedometer scale factor
\mathbf{r}	rover position vector
r	magnitude of rover position vector
R_m	radius of planet (Mars)
σ_α^2	initial pitch variance
SF_v	speedometer scale factor
σ_γ^2	initial heading variance (bias squared)
σ_h^2	initial altitude variance (bias squared)
$\sigma_{h\alpha}^2$	initial pitch/altitude covariance
τ_α	pitch error model time constant
τ_f	vector of the three accelerometer bias time constants
τ_γ	heading error model time constant
τ_h	altitude error time constant for IMU case
τ_v	speedometer error model time constant
\mathbf{v}	vector of three gyroscope drift rates
v_x	gyroscope drift about the x (East) axis
v_x	gyroscope drift about the z (South) axis
v_y	gyroscope drift about the y (Up) axis
v	speed
\mathbf{v}	velocity vector
v_E	component of rover planet-relative velocity in East direction
v_S	component of rover planet-relative velocity in South direction
v_U	component of rover planet-relative velocity in Up direction

ω	planet (Mars) spin rate
ω_{im}^i	planet spin vector in inertial coordinates
ω_{im}^n	planet spin vector in navigation coordinates
ω_{nm}^n	rotation vector of navigation with respected to Mars-fixed frames
\mathbf{x}	rover state vector (position and velocity)
Ψ	vector of three IMU misalignment angles
Ψ_x	IMU misalignment angle about the x (East) axis
Ψ_y	IMU misalignment angle about the y (Up) axis
Ψ_z	IMU misalignment angle about the z (South) axis

Appendix C: Values of Physical Constants

π	3.1415926535897932358
g	9.80665 m/s ²
c	299,792,500 m/s
R_m	3,393,400 m
μ_m	4.282844 x 10 ¹³ m ³ /s ²
ω	7.08821766 x 10 ⁻⁵ rad/s